Simulations of water-vapor two-phase flows with non-condensable gas using a Noble-Able-Chemkin equation of state

Olivier Hurisse, Lucie Quibel

Simulations of water-vapor two-phase flows with non-condensable gas using a Noble-Able-Chemkin equation of state.

Olivier Hurisse[a,], Lucie Quibel[a,b,*]

[a]*EDF R&D, 6 quai Watier, 78400 Chatou, France.*
[b]*IRMA, UMR CNRS 7501, 7 rue Descartes, 67000 Strasbourg, France.*

Abstract

In order to simulate some accidental scenarii which might affect a pressurized water reactor, a homogeneous two-phase water-vapor flow model taking into account noncondensable gas is considered. The liquid phase and the gaseous phase are assumed to be immiscible, but the gaseous phase is composed of two miscible components. Due to these hybrid hypotheses of miscibility, the configurations with at least one missing field are carefully examined. A semi-analytical equation of state is chosen for the liquid water, which is an extension of the Noble-Able stiffened gas equation of state. Its accuracy is assessed with respect to the reference equation of state IAPWS. The homogeneous model is first verified thanks to Riemann problems. Then, some simulations aiming at reproducing SUPERCANON experiment are presented. The amount of air dissolved in liquid water is shown to have a strong influence on numerical results, in particular on the sound speed. Some out of thermodynamical equilibrium simulations are also presented, using two time scales describing the return towards equilibrium.

Key words: Two-phase flow, mass transfer, Look-up table, Nucleation

*Corresponding author
Email addresses: olivier.hurisse@edf.fr (Olivier Hurisse), lucie.quibel@edf.fr (Lucie Quibel)

Introduction

In the framework of nuclear safety demonstration for pressurized water reactors, some accidental scenarii are studied (see IRSN website (1)). For instance, in case of loss of coolant accident (LOCA), pressurized water may undergo a brutal depressurization, leading to a rapid mass transfer. Such scenarii involve complex compressible two-phase flow mixtures, undergoing fast transient situations with phase transition. In addition to liquid and vapor water, other gases may be present: indeed, ambiant air may be mixed with vapor through the free surface of water, or hydrogen might appear under accidental conditions because of fuel oxydation. The proportion of non-condensable gas compared with water vapor is a parameter of importance, appearing to limit the steam condensation, as it has been beared out by experimental studies (2) as well as numerical studies (3). Non-condensable gas is classically taken into account in the reference industrial codes used to simulate a vapor explosion (4; 5).

The flows of interest in this work are thus mixtures of the two following components:

- a liquid and its associated vapor (water is considered in the following), with phase transition which may occur between both phases;
- non-condensable gas, such as air.

Many models have been proposed since decades to simulate two-phase flow mixtures of liquid and vapor water. One may distinguish two main types of models:

- the so-called two-fluid model as those proposed in (6; 7; 8; 9; 10), where each phase is described by its own velocity and where the full thermodynamical disequilibrium is accounted for, in terms of pressure, temperature and chemical potential;
- the so-called homogeneous models, where all the fields have the same velocity; often, at least one additional equilibrium assumption is made (in terms of pressure, temperature...), as in (11; 12; 13; 14; 15; 16; 17)) , whereas there is no other equilibrium assumption in the model proposed in (18).

Both strategies are of interest and the choice between one or the other type of model should be made depending on the targeted applications. For instance, when dealing with accidental scenarii such as vapor explosion, evaluating the velocity gaps between phases is very important to correctly take into account the interfacial transfers due to the dislocation of droplets, driving the heat transfer between phases (see (19; 4)). However, in terms of numerical costs, the two-velocity assumption imposes more constraints on mesh cell size, compared with an homogeneous approach, which may be restrictive for some industrial simulations.

Less references exist for two-phase flow mixtures involving an additional inert gas. Still, the same classification arises, and two-fluid-type models dealing with liquid water and miscible mixtures of steam water and gas have been proposed in (20) or (21). Here, we choose to work on a direct extension of the homogeneous two-phase flow model proposed in (18) and studied for instance in (22; 23). Note that a homogeneous three-phase flow model, also based on (18), has been built in (24), to deal with immiscible mixtures of three fields: we need in our present case a model tackling both miscible and immiscible phases. The main difficulty when dealing with such homogeneous models is to build consistent thermodynamical quantities as well as a mixture equation of state complying with the second law of thermodynamics.

Such a work has been already done in (25) for a homogeneous model with non-condensable gas. In this reference, the associated HEM model is first studied; then, two HRM models are proposed: a model without phase transition with an equilibrium in terms of chemical potential as well as a HRM model with no further equilibrium assumption than the kinematic equilibrium. The associated HEM model had been already simulated in (3), by taking advantage of some particular properties of the model equipped with stiffened gas phasic equations of state (EOS): with this particular choice for phasic EOS, the obtained mixture EOS is indeed very simple since it can be written itself as a

stiffened gas EOS with coefficients depending on the non-condensable gas fraction.

In this work, we first detail in section 1 the modelling approach leading to the second HRM model introduced in (25). This model copes with full disequilibrium mixtures in terms of pressure, temperature and chemical potentials: the only equilibrium assumption is the kinematic equilibrium. The main contribution of the present work is then to propose some numerical simulations based on this model, using a realistic EOS for the liquid water : a Noble-Able Stiffened Gas (NASG) EOS (26), modified with the Chemkin EOS (27), as proposed in (28), called NASG-CK EOS in the sequel and described in section 2. Our numerical method, briefly recalled in section 3, relies on finite volumes convective schemes and has already been implemented in similar contexts for instance in (22; 23): we insist here above all on the thermodynamical equilibrium computation, somehow tricky due to the presence of the non-condensable gas. Note that another numerical work based on the same model has been proposed in (29) using stiffened gas EOS, but dealing with Lattice-Boltzmann method. Last, numerical results are presented: first, the code is assessed by convergence studies on several Riemann problems in section 4; then, some validation cases are presented in section 5.

1 Homogeneous two-phase flow model with non-condensable gas

In this section, the homogeneous model used in this work is presented. It has been built following a similar approach as the one depicted for instance in (18; 23; 24). That is why only the main features of the model are recalled here. In particular, we insist on the miscibility assumptions as well as on the thermodynamical building, which are the less classical parts of the modelling.

For sake of readibility, a field will be designated by a subscript $k \in \mathcal{K} = \{l, v, a\}$, with l refering to liquid water, v to water vapor and a to non-condensable gas.

1.1 *Kinematic equilibrium and general assumptions*

Hypothesis 1 —

Kinematic equilibrium is assumed in the model for all fields. As a consequence, there is only one velocity U ($m.s^{-1}$) in the model, so that:

$$U = U_l = U_v = U_a. \tag{1}$$

It implies that the derivative of a given quantity Φ along a streamline does not depend on the subscript $k \in \mathcal{K}$:

$$\begin{aligned} d_k\Phi &= (\partial_t\Phi + U_k\partial_x\Phi)\, dt \\ &= (\partial_t\Phi + U\partial_x\Phi)\, dt = d\Phi. \end{aligned} \tag{2}$$

Note that only the kinematic equilibrium is assumed: all the other quantities (such pressures or temperatures) may be different for each field.

Moreover, the following simplifying assumptions are made:

Hypothesis 2 —

The exact geometric repartition of each field in a given amount of mixture is not known and the surface tension is neglected.

Hypothesis 3 —

Vaccuum occurence is not considered.

1.2 *Extensive description of the considered flows*

Each field $k \in \mathcal{K}$ can be described thanks to three extensive variables, like for instance in (30): its volume $\mathcal{V}_k \geq 0$ (in m^3), its mass $\mathcal{M}_k \geq 0$ (in kg) and its internal energy $\mathcal{E}_k$ (in J). Similarly, the entire mixture can be depicted by its volume $\mathcal{V} > 0$ (in m^3), its mass $\mathcal{M} > 0$ (in kg) and its internal energy $\mathcal{E} \neq 0$ (in J). In the following, we note:

$$\Omega_k = \{W_k = (\mathcal{V}_k, \mathcal{M}_k, \mathcal{E}_k) \ / \ \mathcal{V}_k \geq 0, \mathcal{M}_k \geq 0\};;$$

$$\Omega = \{W = (\mathcal{V}, \mathcal{M}, \mathcal{E}) \ / \ \mathcal{V} > 0, \mathcal{M} > 0\},$$

$$\widetilde{\Omega_{lva}} = \{W_{lva} = (W_l, W_v, W_a) \ / \ \forall k \in \mathcal{K}, W_k \in \Omega_k\}.$$

Remark 1 — Hypothesis 3 implies that there exists at least one subscript $k \in \mathcal{K}$ so that : $\Omega_k = \{W_k = (\mathcal{V}_k, \mathcal{M}_k, \mathcal{E}_k) \ / \ \mathcal{V}_k > 0 \text{ and } \mathcal{M}_k > 0\}$.

1.2.1 Hybrid miscibility conditions

Hypothesis 4 (Miscibility constraints) —
Considering a given amount of fluid characterized by $W = (\mathcal{V}, \mathcal{M}, \mathcal{E}) \in \Omega$, it can be depicted as a mixture of two **immiscible** phases:

- a liquid phase with only liquid water;
- a gaseous phase (designated by the subscript g), which is a **miscible** mixture of water vapor and non-condensable gas.

Thanks to hypothesis 2, ideal miscibility and immiscibility conditions can be written, as proposed for instance in (31). The miscibility condition for the gaseous phase leads to:

$$\begin{cases} \mathcal{V}_g = \mathcal{V}_v = \mathcal{V}_a; \\ \mathcal{M}_g = \mathcal{M}_v + \mathcal{M}_a; \\ \mathcal{E}_g = \mathcal{E}_v + \mathcal{E}_a, \end{cases} \tag{3}$$

whereas the immiscibility condition for the liquid-gas mixture leads to:

$$\begin{cases} \mathcal{V} = \mathcal{V}_l + \mathcal{V}_g; \\ \mathcal{M} = \mathcal{M}_l + \mathcal{M}_g; \\ \mathcal{E} = \mathcal{E}_l + \mathcal{E}_g, \end{cases} \tag{4}$$

Relations (3) and (4) can be rewritten with only subscripts in $\mathcal{K}$ as:

$$\begin{cases} \mathcal{V} = \mathcal{V}_l + \mathcal{V}_v = \mathcal{V}_l + \mathcal{V}_a; \\ \mathcal{M} = \mathcal{M}_l + \mathcal{M}_v + \mathcal{M}_a; \\ \mathcal{E} = \mathcal{E}_l + \mathcal{E}_v + \mathcal{E}_a. \end{cases} \tag{5}$$

Then, considering $W = (\mathcal{V}, \mathcal{M}, \mathcal{E}) \in \Omega$, we note $\Omega_{lva}(W)$ the subset of all the mixtures characterized by W verifying the miscibility conditions (5), i.e.:

$$\begin{aligned}\Omega_{lva}(W) = \quad & \{W_{lva} \in \widetilde{\Omega_{lva}} / \\ & \mathcal{V} = \mathcal{V}_l + \mathcal{V}_v = \mathcal{V}_l + \mathcal{V}_a, \\ & \mathcal{M} = \mathcal{M}_l + \mathcal{M}_v + \mathcal{M}_a, \\ & \mathcal{E} = \mathcal{E}_l + \mathcal{E}_v + \mathcal{E}_a.\}.\end{aligned}$$

Moreover, since a is a non-condensable gas, the following hypothesis holds:

Hypothesis 5 —
A mass of non-condensable gas $\mathcal{M}_a$ is only convected within the flow. Then, when considering a fixed mass of mixture $\mathcal{M} = \mathcal{M}_l + \mathcal{M}_v + \mathcal{M}_a$ (i.e. a closed system), the mass of non-condensable gas $\mathcal{M}_a$ inside $\mathcal{M}$ remains constant within time:

$$d\mathcal{M} = 0 \quad \Longrightarrow \quad d\mathcal{M}_a = 0 \ \ \& \ \ d\mathcal{M}_l = -d\mathcal{M}_v.$$

Remark 2 — Note that conditions (4) are exactly those considered when building the model (18) from extensive variables in (23), except that the gaseous phase is now a miscible mixture of vapor and non-condensable gas, instead of pure vapor.

Last, we introduce the phasic fractions, which will be very useful in the following. For any $k \in \mathcal{K}$, we note α_k the volume fraction of the field k within the flow, y_k the mass fraction and z_k the energy fraction, defined as follows:

$$\alpha_k = \frac{\mathcal{V}_k}{\mathcal{V}} \quad ; \quad y_k = \frac{\mathcal{M}_k}{\mathcal{M}} \quad ; \quad z_k = \frac{\mathcal{E}_k}{\mathcal{E}}. \tag{6}$$

Relation (5) can be rewritten as:

$$\begin{cases} 1 = \alpha_l + \alpha_v & \text{and} \quad \alpha_v = \alpha_a; \\ 1 = y_l + y_v + y_a; & \\ 1 = z_l + z_v + z_a. & \end{cases} \tag{7}$$

Thanks to the miscibility constraints (7), only one volume fraction, two mass fractions and two energy fractions are required to completely describe the system. In the following, we arbitrarily choose α_v, y_v, y_a, z_v and z_a. The liquid fractions are then deduced from the gaseous fractions and from (7).

Hypothesis 6 (Monophasic cases) —
One phase or one field may be absent:

- if water vapor v (respectively non-condensable gas a) is absent, then $\mathcal{M}_v = 0$, $\mathcal{V}_v = 0$ and $\mathcal{E}_v = 0$ (resp. $\mathcal{M}_a = 0$, $\mathcal{V}_a = 0$ and $\mathcal{E}_a = 0$), so that conditions (5) and (7) become for all $k \in \{v, a\}$:

$$\begin{cases} \mathcal{V} = \mathcal{V}_l + \mathcal{V}_k; \\ \mathcal{M} = \mathcal{M}_l + \mathcal{M}_k; \\ \mathcal{E} = \mathcal{E}_l + \mathcal{E}_k; \end{cases} \tag{8}$$

  and

$$\begin{cases} 1 = \alpha_l + \alpha_k; \\ 1 = y_l + y_k; \\ 1 = z_l + z_k. \end{cases} \tag{9}$$

- if liquid water is absent, then $\mathcal{M}_l = 0$, $\mathcal{V}_l = 0$ and $\mathcal{E}_l \neq 0$, so that conditions (5) and (7) become:

$$\begin{cases} \mathcal{V} = \mathcal{V}_v = \mathcal{V}_a; \\ \mathcal{M} = \mathcal{M}_v + \mathcal{M}_a; \\ \mathcal{E} = \mathcal{E}_v + \mathcal{E}_a; \end{cases} \tag{10}$$

  and

$$\begin{cases} 1 = \alpha_v = \alpha_a; \\ 1 = y_v + y_a; \\ 1 = z_v + z_a. \end{cases} \tag{11}$$

- pure monophasic cases l, v or a are also possible:

$$\exists k \in \{l, v, a\}, \alpha_k = y_k = z_k = 1. \tag{12}$$

The states with only l and a or the states with only v and a lead to degenerate equilibrium hypotheses that will be described in property 4.

1.2.2 Chosen approach in order to derive the equations

The same approach as (24; 23) (among other references) is used to derive the model equations. A given amount of fluid characterized by the mixture quantities $W = (\mathcal{V}, \mathcal{M}, \mathcal{E}) \in \Omega$ is considered. By adopting a Lagrangian point of view, the modelling is proceeded in two steps:

1. first, the fluid element is considered as fixed, closed and isolated from the rest of the flow: its evolution should comply with the second law of thermodynamics;
2. then, the interaction with the surrounding fluid is considered: the fluid element should evolve within time in accordance with Newton laws and the first law of thermodynamics.

The second step is exactly the same as the one used for instance in (24; 23): the approach leads to depict the mixture by Euler-type equations for the mixture quantities, i.e. density, momentum and total energy. The reader can refer to the previous references or to (18; 32; 33; 34; 35; 30; 22; 24) to have more details. We only highlight that hypothesis 1 and operator (2) are the key ingredients to derive the equations.

The first step allows to properly define the mixture thermodynamical quantities such as pressure and to build equations and source terms enabling to return towards the thermodynamical equilibrium within time. The thermodynamical behavior of the considered mixtures of l, v and a with hybrid miscibility constraints has already been studied in (25). In the sequel of the section, we will derive a similar approach, adapted to our model framework.

1.2.3 *Equation of state (EOS) for each field*

In order to close the system, a complete equation of state (EOS) is required for each field $k \in \mathcal{K}$. As in (22; 24; 23), a natural way to define such an EOS is to consider an extensive entropy $W_k \in \Omega_k \mapsto S_k(W_k)$ (in $J.K^{-1}$) as thermodynamical potential for each field $k \in \mathcal{K}$, with $W_k = (\mathcal{V}_k, \mathcal{M}_k, \mathcal{E}_k)$.

In order to ensure the hyperbolicity of the final model, some properties are required for each k-field EOS $W_k \in \Omega_k \mapsto S_k(W_k)$ (see section 1.4).

Property 1 (Required properties for S_k)
A k-field EOS $W_k \in \Omega_k \mapsto S_k(W_k)$ is an admissible EOS ensuring the hyperbolicity of the final model (see (24; 23) and section 1.4) if the following properties hold:

$$
\begin{aligned}
&(I) \quad W_k \in \Omega_k \mapsto S_k(W_k) \text{ is } \mathcal{C}^2.\\
&(II) \quad W_k \in \Omega_k \mapsto S_k(W_k) \text{ is concave.}\\
&(III) \quad \forall a \in \mathbb{R}^+, \forall W_k \in \Omega_k,\ S_k(aW_k) = aS_k(W_k).\\
&(IV) \quad \forall W_k \in \Omega_k,\ \left.\frac{\partial S_k}{\partial \mathcal{E}_k}\right|_{\mathcal{V}_k,\mathcal{E}_k} > 0.
\end{aligned}
$$

In agreement with the Classical Irreversible Thermodynamics (CIT) theory, the classical Gibbs relation holds for each field $k \in \mathcal{K}$:

$$T_k d_k \mathcal{S}_k = d_k \mathcal{E}_k + P_k d_k \mathcal{V}_k - \mu_k d_k \mathcal{M}_k, \tag{13}$$

which can be rewritten thanks to (2) as:

$$T_k d \mathcal{S}_k = d \mathcal{E}_k + P_k d \mathcal{V}_k - \mu_k d \mathcal{M}_k. \tag{14}$$

Since $S_k(\mathcal{V}_k, \mathcal{M}_k, \mathcal{E}_k)$ is a complete EOS for field k, all the thermodynamical quantitites can be computed thanks to the derivatives of S_k.

Definition 1 (Phasic quantities for a *k*-field)

Considering a field $k \in \mathcal{K}$, its pressure P_k (in Pa), its temperature T_k (in K) and its Gibbs free enthalpy μ_k (in $J.kg^{-1}$) can be derived in accordance with the chosen complete EOS $W_k \in \Omega_k \mapsto S_k(W_k)$, thanks to the Gibbs relation (14):

$$\frac{P_k}{T_k} = \left.\frac{\partial S_k}{\partial \mathcal{V}_k}\right|_{\mathcal{M}_k, \mathcal{E}_k}, \tag{15}$$

$$\frac{1}{T_k} = \left.\frac{\partial S_k}{\partial \mathcal{E}_k}\right|_{\mathcal{V}_k, \mathcal{M}_k} > 0, \tag{16}$$

$$\frac{\mu_k}{T_k} = -\left.\frac{\partial S_k}{\partial \mathcal{M}_k}\right|_{\mathcal{V}_k, \mathcal{E}_k}. \tag{17}$$

1.2.4 Defining the thermodynamical quantities for the mixture

Definition 2 (Mixture entropy *S*)

Recalling that $W_k = (\mathcal{V}_k, \mathcal{M}_k, \mathcal{E}_k) \in \Omega_k$, we consider $W_{lva} = (W_l, W_v, W_a)$ and $W = (\mathcal{V}, \mathcal{M}, \mathcal{E}) \in \Omega$ so that $W_{lva} \in \Omega_{lva}(W)$. As in (25), we define the entropy of the mixture S as:

$$W \in \Omega \mapsto S(W) = S_l(W_l) + S_v(W_v) + S_a(W_a). \tag{18}$$

Note that the previous definition of the mixture entropy (18) is in accordance with the ideal miscibility conditions (5) that we have previously assumed. However, it should be modified if surface tension (or other effects, see (10)) had to be accounted for.

From (18) and (14) and using operator (2), a Gibbs relation for the mixture entropy S can be derived after simple computations using the relation $d\Phi_k = \Phi d\left(\frac{\Phi_k}{\Phi}\right) + \frac{\Phi_k}{\Phi} d\Phi$ and the definition of the fractions (6).

Definition 3 (Mixture quantities)

A mixture pressure P (Pa), a mixture temperature T (in K) and a mixture Gibbs enthalpy μ (in $J.kg^{-1}$) can be exhibited by identifying them in the following mixture Gibbs relation:

$$\begin{aligned} dS &= \frac{1}{T}\left(Pd\mathcal{V} - \mu d\mathcal{M} + d\mathcal{E}\right) \\ &+ \mathcal{V}\sum_{k\in\mathcal{K}}\frac{P_k}{T_k}d\alpha_k \\ &- \mathcal{M}\sum_{k\in\mathcal{K}}\frac{\mu_k}{T_k}dy_k \\ &+ \mathcal{E}\sum_{k\in\mathcal{K}}\frac{1}{T_k}dz_k. \end{aligned} \tag{19}$$

They read:

$$\frac{P}{T} = \sum_{k\in\mathcal{K}}\alpha_k\frac{P_k}{T_k}, \tag{20}$$

$$\frac{\mu}{T} = \sum_{k\in\mathcal{K}}y_k\frac{\mu_k}{T_k}, \tag{21}$$

$$\frac{1}{T} = \sum_{k\in\mathcal{K}}z_k\frac{1}{T_k}. \tag{22}$$

We interpret Gibbs relation (19) as follows:

- the first part $\frac{1}{T}\left(Pd\mathcal{V} - \mu d\mathcal{M} + d\mathcal{E}\right)$ gathers terms due to the mixture itself; they vanish when the flow element is considered as fixed ($d\mathcal{V} = 0$), closed ($d\mathcal{M} = 0$) and isolated ($d\mathcal{E} = 0$) from the rest of the flows, as it will be studied in section 1.2.5.
- the second part $\mathcal{V}\sum_{k\in\mathcal{K}}\frac{P_k}{T_k}d\alpha_k - \mathcal{M}\sum_{k\in\mathcal{K}}\frac{\mu_k}{T_k}dy_k + \mathcal{E}\sum_{k\in\mathcal{K}}\frac{1}{T_k}dz_k$ gather exchange terms between the three fields within the mixture.

1.2.5 Second law of thermodynamics and thermodynamical equilibrium

In this section we consider a closed system isolated from the rest of the flow : a fixed amount of mixture characterized by $W = (\mathcal{V}, \mathcal{M}, \mathcal{E}) \in \Omega$. It implies now:

$$d\mathcal{V} = 0 \quad ; \quad d\mathcal{M} = 0 \quad ; \quad d\mathcal{E} = 0.$$

More precisely, we consider all the physical states $W_{lva} = (W_l, W_v, W_a) \in \Omega_{lva}(W)$.

Recalling the hypothesis 5 due to the non-condensable gas, we have $d\mathcal{M}_a = 0$ and $d\mathcal{M}_l = -d\mathcal{M}_v$, i.e.:

$$dy_a = 0 \quad \text{and} \quad dy_l = -dy_v.$$

Moreover, thanks to the miscibility conditions (5), Gibbs relation can be rewritten as a function of α_v, y_v, y_a, z_v and z_a, since:

$$\alpha_l = 1 - \alpha_v \quad \text{and} \quad \alpha_v = \alpha_a;$$

$$y_l = 1 - y_v - y_a;$$

$$z_l = 1 - z_v - z_a.$$

Then, for the considered isolated system, Gibbs relation (19) can be simplified as follows:

$$\begin{aligned} dS \;=\; & \mathcal{V}\left(\left(\frac{P_v}{T_v} + \frac{P_a}{T_a}\right) - \frac{P_l}{T_l}\right) d\alpha_v \\ + \; & \mathcal{M}\left(\frac{\mu_l}{T_l} - \frac{\mu_v}{T_v}\right) dy_v \\ + \; & \mathcal{E}\left(\frac{1}{T_v} - \frac{1}{T_l}\right) dz_v + \mathcal{E}\left(\frac{1}{T_a} - \frac{1}{T_l}\right) dz_a, \end{aligned} \tag{23}$$

and relations (20) and (22) becomes:

$$P(Y, \tau, e) = \frac{(1-\alpha_v)\frac{P_l}{T_l} + \alpha_v\left(\frac{P_v}{T_v} + \frac{P_a}{T_a}\right)}{\frac{1-z_v-z_a}{T_l} + \frac{z_v}{T_v} + \frac{z_a}{T_a}}; \tag{24}$$

$$\frac{1}{T}(Y, \tau, e) = \frac{1-z_v-z_a}{T_l} + \frac{z_v}{T_v} + \frac{z_a}{T_a}. \tag{25}$$

In order to comply with the second law of thermodynamics, we have to postulate some form for $d\alpha_k$, dy_k and dz_k, ensuring that the mixture entropy will increase for the considered isolated system, i.e. so that $dS \geq 0$, with dS defined through the Gibbs relation (23).

Hypothesis 7 —

As initially proposed in (18), we assume the following time evolution for the fractions:

$$\begin{cases} \forall k \in \mathcal{K},\ d\alpha_k = \dfrac{\bar{\alpha_k} - \alpha_k}{\lambda} \\ \forall k \in \{l, v\},\ dy_k = \dfrac{\bar{y_k} - y_k}{\lambda} \quad \text{and} \quad dy_a = 0, \\ \forall k \in \mathcal{K},\ dz_k = \dfrac{\bar{z_k} - z_k}{\lambda}, \end{cases} \tag{26}$$

where $\lambda > 0$ and for all $k \in \mathcal{K}$, $\bar{\alpha_k} = \dfrac{\bar{V_k}}{V}$, $\bar{y_k} = \dfrac{\bar{M_k}}{M}$ and $\bar{z_k} = \dfrac{\bar{E_k}}{E}$, with $\bar{W}_{lva} = (\bar{W}_l, \bar{W}_v, \bar{W}_a) \in \Omega_{lva}(W)$ the state that the system will asymptotically reach within time. Note that λ may be defined as a function of time, of space, of W... The only constraint on λ is its positivity:

$$\lambda > 0.$$

Property 2 (Concavity of S)

S is strictly concave on $\Omega_{lva}(W)$. More details are given in appendix 6.

Property 3

If $\bar{W}_{lva}$ is defined as the maximum of the mixture entropy S (which exists and is unique thanks to the strict concavity of S), then the second law is ensured. If the equilibrium state $\bar{W}_{lva}$ is not reached on a border of $\Omega_{lva}(W)$ (that is to say, if $\bar{W}_{lva}$ is a two-phase mixture with all the three fields l, v and a), $\bar{W}_{lva}$ can be characterized by the first order conditions for the existence of extremums, that give here:

$$\begin{cases} T_l(\bar{\mathcal{V}}_l, \bar{\mathcal{M}}_l, \bar{\mathcal{E}}_l) = T_v(\bar{\mathcal{V}}_v, \bar{\mathcal{M}}_v, \bar{\mathcal{E}}_v) = T_a(\bar{\mathcal{V}}_a, \bar{\mathcal{M}}_a, \bar{\mathcal{E}}_a) \\ P_l(\bar{\mathcal{V}}_l, \bar{\mathcal{M}}_l, \bar{\mathcal{E}}_l) = P_v(\bar{\mathcal{V}}_v, \bar{\mathcal{M}}_v, \bar{\mathcal{E}}_v) + P_a(\bar{\mathcal{V}}_a, \bar{\mathcal{M}}_a, \bar{\mathcal{E}}_a) \\ \mu_l(\bar{\mathcal{V}}_l, \bar{\mathcal{M}}_l, \bar{\mathcal{E}}_l) = \mu_v(\bar{\mathcal{V}}_v, \bar{\mathcal{M}}_v, \bar{\mathcal{E}}_v). \end{cases} \tag{27}$$

The second equilibrium condition (i.e. for the pressures) coincides with the Dalton law.

Property 4 (Equilibrium states & missing fields)
The thermodynamical equilibrium may be reached on a border of $\Omega_{lva}(W)$ and then, conditions (27) are no longer relevant. Depending on the present components, the following conditions should be used to determine the thermodynamical equilibrium:

- with a two-phase mixture of liquid and steam water: the same conditions as for instance (22; 23) hold:

$$\begin{cases} T_l(\bar{\mathcal{V}}_l, \bar{\mathcal{M}}_l, \bar{\mathcal{E}}_l) = T_v(\bar{\mathcal{V}}_v, \bar{\mathcal{M}}_v, \bar{\mathcal{E}}_v) \\ P_l(\bar{\mathcal{V}}_l, \bar{\mathcal{M}}_l, \bar{\mathcal{E}}_l) = P_v(\bar{\mathcal{V}}_v, \bar{\mathcal{M}}_v, \bar{\mathcal{E}}_v) \\ \mu_l(\bar{\mathcal{V}}_l, \bar{\mathcal{M}}_l, \bar{\mathcal{E}}_l) = \mu_v(\bar{\mathcal{V}}_v, \bar{\mathcal{M}}_v, \bar{\mathcal{E}}_v). \end{cases} \tag{28}$$

- with a non-miscible two-phase mixture of liquid water and non-condensable gas (l and a), the following conditions hold, since no phase transition occurs:

$$\begin{cases} T_l(\bar{\mathcal{V}}_l, \bar{\mathcal{M}}_l, \bar{\mathcal{E}}_l) = T_a(\bar{\mathcal{V}}_a, \bar{\mathcal{M}}_a, \bar{\mathcal{E}}_a) \\ P_l(\bar{\mathcal{V}}_l, \bar{\mathcal{M}}_l, \bar{\mathcal{E}}_l) = P_a(\bar{\mathcal{V}}_a, \bar{\mathcal{M}}_a, \bar{\mathcal{E}}_a). \end{cases} \tag{29}$$

- with a miscible monophasic gaseous mixture of water vapor and non-condensable gas (v and a), only one condition remains:

$$T_v(\bar{\mathcal{V}}_v, \bar{\mathcal{M}}_v, \bar{\mathcal{E}}_v) = T_a(\bar{\mathcal{V}}_a, \bar{\mathcal{M}}_a, \bar{\mathcal{E}}_a). \tag{30}$$

1.3 Final system of equations

1.3.1 Intensive quantities

We introduce some notations for the intensive quantities:

- $\rho = \frac{\mathcal{M}}{\mathcal{V}}$ stands for the density (in $kg.m^{-3}$);
- $\tau = \frac{1}{\rho} = \frac{\mathcal{V}}{\mathcal{M}}$ for the specific volume;
- $e = \frac{\mathcal{E}}{\mathcal{M}}$ stands for the specific internal energy (in $J.kg^{-1}$), $E = e + \frac{1}{2}|U|^2$ for the total specific energy;

- $s = \frac{\mathcal{S}}{\mathcal{M}}$ stands for the specific entropy (in $J.K^{-1}.kg^{-1}$).

A quantity Φ without a subscript designates a mixture quantity, whereas a quantity Φ_k refers to field $k \in \mathcal{K}$.

1.3.2 Final system of partial differential equations (PDE)

Eventually, the model can be written with the intensive variables, by applying Newton laws and first law of thermodynamics (see (23)) and by using the source terms (26) exhibited in the previous section:

$$\left\{\begin{array}{l}
\frac{\partial}{\partial t}(\rho\alpha_v) + \frac{\partial}{\partial x}(\rho U\alpha_v) = \rho\frac{(\bar{\alpha_v} - \alpha_v)}{\lambda}, \\
\frac{\partial}{\partial t}(\rho y_v) + \frac{\partial}{\partial x}(\rho U y_v) = \rho\frac{(\bar{y_v} - y_v)}{\lambda}, \\
\frac{\partial}{\partial t}(\rho y_a) + \frac{\partial}{\partial x}(\rho U y_a) = 0, \\
\frac{\partial}{\partial t}(\rho z_v) + \frac{\partial}{\partial x}(\rho U z_v) = \rho\frac{(\bar{z_v} - z_v)}{\lambda}, \\
\frac{\partial}{\partial t}(\rho z_a) + \frac{\partial}{\partial x}(\rho U z_a) = \rho\frac{(\bar{z_a} - z_a)}{\lambda}, \\
\frac{\partial}{\partial t}(\rho) + \frac{\partial}{\partial x}(\rho U) = 0, \\
\frac{\partial}{\partial t}(\rho U) + \frac{\partial}{\partial x}(\rho U^2 + P) = 0, \\
\frac{\partial}{\partial t}(\rho E) + \frac{\partial}{\partial x}(U(\rho E + P)) = 0.
\end{array}\right. \tag{31}$$

We note $Y = (\alpha_v, y_v, y_a, z_v, z_a)$ and we recall the constraints that give α_l, y_l and z_l from Y:

$$\left\{\begin{array}{rcll}
1 &=& \alpha_l + \alpha_v & \& \quad \alpha_v = \alpha_a; \\
1 &=& y_l + y_v + y_a; & \\
1 &=& z_l + z_v + z_a. &
\end{array}\right.$$

Some useful relations between mixture and phasic quantities can be written:

$$\forall k \in \mathcal{K}, \quad \tau_k = \frac{\alpha_k}{y_k}\tau \quad ; \quad e_k = \frac{z_k}{y_k}e. \tag{32}$$

In order to close system (31), the user must specify one equation of state for each field k (see section 2) and a time-scale $\lambda > 0$ describing the return to the thermodynamical

equilibrium. For the latter, few references exist in the litterature to estimate λ based on physical considerations. For instance, in (23), a proposition has been made, by considering time scales from nucleation theory.

The definitions of the thermodynamical quantities introduced in the previous section are rewritten with intensive variables. First, Gibbs relation for a field $k \in \mathcal{K}$ reads:

$$T_k ds_k = de_k + P_k d\tau_k, \tag{33}$$

where

$$\frac{1}{T_k} = \left.\frac{\partial s_k}{\partial e_k}\right|_{\tau_k} \quad ; \quad \frac{P_k}{T_k} = \left.\frac{\partial s_k}{\partial \tau_k}\right|_{e_k}. \tag{34}$$

Moreover, we recall the definition of the chemical potential μ_k:

$$\mu_k = e_k - T_k s_k + P_k \tau_k. \tag{35}$$

The mixture entropy definition (18) becomes:

$$s(Y, \tau, e) = (1 - y_v - y_a) s_l(\tau_l, e_l) + y_v s_v(\tau_v, e_v) + y_a s_a(\tau_a, e_a), \tag{36}$$

so that the mixture Gibbs relation (19) gives, since $d\mathcal{M} = 0$:

$$\begin{aligned} ds &= \frac{1}{T}\left(P d\tau + de\right) + \tau\left(\left(\frac{P_v}{T_v} + \frac{P_a}{T_a}\right) - \frac{P_l}{T_l}\right) d\alpha_v \\ &+ \left(\frac{\mu_l}{T_l} - \frac{\mu_v}{T_v}\right) dy_v \\ &+ e\left(\frac{1}{T_v} - \frac{1}{T_l}\right) dz_v + e\left(\frac{1}{T_a} - \frac{1}{T_l}\right) dz_a, \end{aligned} \tag{37}$$

where:

$$P(Y, \tau, e) = \frac{(1 - \alpha_v)\frac{P_l}{T_l} + \alpha_v\left(\frac{P_v}{T_v} + \frac{P_a}{T_a}\right)}{\frac{1 - z_v - z_a}{T_l} + \frac{z_v}{T_v} + \frac{z_a}{T_a}}; \tag{38}$$

$$\frac{1}{T}(Y, \tau, e) = \frac{1 - z_v - z_a}{T_l} + \frac{z_v}{T_v} + \frac{z_a}{T_a}. \tag{39}$$

Some concavity properties can be exhibited for the entropy: s is strictly concave relatively to Y for a given (τ, e) and s is strictly concave relatively to (τ, e) for a given Y (see appendix 6).

1.4 Main properties of the model

The present model possesses interesting mathetical properties. They are only summarized here but the reader can refer to (18; 32; 33; 34; 35; 30; 22; 24) for more details about models with a similar convective structure and to (25) for details about a homogeneous model with the same thermodynamical building.

Property 5 (Maximum principle on fractions)
If:

(I) : initial and boundary conditions on fractions are so that $Y^0 \in [0,1]^5$;

(II) : equilibrium fractions $\bar{Y}$ are so that $\bar{Y} \in [0,1]^5$;

then the fractions remain in $[0,1]^5$. This property can be proved thanks to the classical lemma recalled in (36).

Let us recall the definition of the mixture sound speed c ($m.s^{-1}$), which is a useful quantity playing a role in the following properties:

Definition 4 (Mixture sound speed c)

$$\begin{aligned} c^2 &= -\tau^2 \left.\frac{\partial P}{\partial \tau}\right|_{s,Y} = -\tau^2 \left.\frac{\partial P}{\partial \tau}\right|_{e,Y} + \tau^2 P \left.\frac{\partial P}{\partial e}\right|_{\tau,Y} \\ &= -\tau^2 T \left(\left.\frac{\partial^2 s}{\partial \tau^2}\right|_{e,Y} + P^2 \left.\frac{\partial^2 s}{\partial e^2}\right|_{\tau,Y} - 2P \left.\frac{\partial^2 s}{\partial \tau \partial e}\right|_{Y} \right), \end{aligned} \tag{40}$$

which can be rewritten thanks to the partial derivatives of the phasic intensive entropies s_k, since:

$$\begin{aligned} \left.\frac{\partial^2 s}{\partial \tau^2}\right|_{e,Y} &= \sum_{k\in\mathcal{K}} \frac{\alpha_k^2}{y_k} \frac{\partial^2 s_k}{\partial \tau_k^2}; \\ \left.\frac{\partial^2 s}{\partial e^2}\right|_{\tau,Y} &= \sum_{k\in\mathcal{K}} \frac{z_k^2}{y_k} \frac{\partial^2 s_k}{\partial e_k^2}; \\ \left.\frac{\partial^2 s}{\partial \tau \partial e}\right|_{Y} &= \sum_{k\in\mathcal{K}} \frac{\alpha_k z_k}{y_k} \frac{\partial^2 s_k}{\partial \tau_k \partial e_k}. \end{aligned} \tag{41}$$

The sound speed c can also be written from second derivatives of chemical potential μ in (P,T)-plane (see (37)):

$$\begin{aligned} c^2 &= -\tau^2 \Big/ \left(\left(\frac{\partial \tau}{\partial P}\right)\Big|_T - \left(\frac{\partial \tau}{\partial T}\right)\Big|_P \frac{\left(\frac{\partial s}{\partial P}\right)\Big|_T}{\left(\frac{\partial s}{\partial T}\right)\Big|_P} \right) \\ &= \left(\frac{\chi_T}{\tau} - \frac{T\alpha_P^2}{C_p} \right)^{-1}, \end{aligned} \tag{42}$$

where $\alpha_P = \dfrac{1}{\tau}\dfrac{\partial^2 \mu}{\partial P \partial T}\Big|_{T,P}$ is the thermal expansion coefficient at constant pressure (K^{-1}) and $\chi_T = -\dfrac{1}{\tau}\dfrac{\partial^2 \mu}{\partial P^2}\Big|_T$ is the compressibility coefficient at constant temperature (Pa^{-1}).

Property 6 (Structure of the waves)

Since system (31) is an Euler-type system, the eigenstructure of the model is composed of:

- two genuinely non-linear waves associated with the eigenvalues $U \pm c$;
- one linearly degenerate wave associated with the eigenvalue U.

Property 7 (Hyperbolicity)

Hyperbolicity is ensured if and only if c is real. From equation (40), the two following conditions are thus sufficient conditions ensuring the hyperbolicity of the model:

(I) : the mixture entropy $(\tau, e) \mapsto s(\tau, e)$ is concave;

(II) : the mixture temperature T is non-negative.

Thanks to (41), (25) and concavity properties of the entropies (see appendix 6 and (24; 23)), the previous conditions can be rewritten as sufficient conditions on phasic Equations Of State (EOS):

Property 8 (Required properties for s_k)

Assuming that $e_k > 0$ (see remark 3), a k-field EOS $(\tau_k, e_k) \mapsto s_k(\tau_k, e_k)$ is an admissible EOS ensuring the hyperbolicity of the final model if the following sufficient properties hold:

$$\begin{aligned} &(I) \quad (\tau_k, e_k) \mapsto s_k(\tau_k, e_k) \text{ is } \mathcal{C}^2. \\ &(II) \quad (\tau_k, e_k) \mapsto s_k(\tau_k, e_k) \text{ is concave.} \\ &(III) \quad \forall (\tau_k, e_k), \ \left.\frac{\partial s_k}{\partial e_k}\right|_{\tau_k} > 0. \end{aligned}$$

Remark 3 — Energy fractions z_k might not satisfy assumptions (I) and (II) in property 5 for some phasic EOS (see remark 4). With $z_k < 0$, we might have a mixture temperature $T < 0$ (and thus a loss of hyperbolicity), even with a phasic EOS satisfying property 8.

Property 9 (Jump conditions)

Shocks are defined in a unique manner through the Rankine-Hugoniot relations:

$$\begin{cases} J[Y] = 0; \\ [J] = 0; \\ J^2[\tau] + [P] = 0; \\ J\left([e] + [\tau]\dfrac{P^L + P^R}{2}\right) = 0, \end{cases} \tag{43}$$

where $J = \rho(U - \sigma)$ with σ the speed of the shock ($\sigma = U - c$ or $\sigma = U + c$) and where $[\Phi] = \Phi^R - \Phi^L$ denotes the difference of the value of the quantity Φ on the right of the discontinuity Φ^R and on the left of the discontinuity Φ^L.

Moreover, for a contact wave, the jump conditions are the following:

$$\begin{cases} [U] = 0; \\ [P] = 0. \end{cases} \tag{44}$$

2 Equations of state (EOS)

The model presented in section 1 requires some thermodynamical closures i.e. one complete phasic EOS for each field l, v and a, verifying the conditions (I)-(III) from property 8. The phasic EOS used in this work are presented here.

We recall that a thermodynamical plane is made up of two intensive physical quantities ϕ_1 and ϕ_2, varying in a domain $\text{dom}(\phi_1, \phi_2)$. An EOS is a function describing a thermodynamical potential Ψ in a thermodynamical plane (ϕ_1, ϕ_2) and an EOS $(\phi_1, \phi_2) \mapsto \Psi(\phi_1, \phi_2)$ is a complete EOS when all the thermodynamical quantities can be defined from the successive derivatives of Ψ with respect to ϕ_1 and ϕ_2. A very comprehensive list of possible thermodynamical potentials can be found in appendix A of (32) and Chapter 2 of (13). In practice, the model of section 1 requires at least **one thermodynamical potential** (described in its natural thermodynamical plane in table 1) and a **compatible change of variables towards another thermodynamical plane**, as it will be explained in more details in section 3. In this work, we need indeed to use the following two thermodynamical planes:

- **the specific entropy s in (τ, e)-plane**: indeed, most classical numerical methods (see section 3.1) require the mixture pressure P, computed with (38) using the phasic pressures and temperatures, themselves obtained from τ_k and e_k (easily deduced from the conservative variables ρ, ρE, $\rho\alpha_k$, ρy_k, ρz_k). Furthermore, this choice allows to handle shock waves with quite simple numerical schemes from conservative variables;
- **the Gibbs potential $\mu = e - Ts + P\tau$ in (P, T)-plane**, since the thermodynamical equilibrium is computed in (P, T)-plane with an algorithm adapted from (14) (see section 3.3).

Some quantities can also be computed with the second derivative of a thermodynamical

potential, for instance, the heat capacity at constant pressure C_p:

$$C_p = -T \left. \frac{\partial^2 \mu}{\partial T^2} \right|_P . \tag{45}$$

Notice that, thanks to assumption (III) of property 8, there is a bijective change of variables to switch from $s(\tau, e)$ towards $e(\tau, s)$ (38; 35).

Potential	Entry plane	"Gibbs relation"	Conjugate variables
μ	(P,T)	$d\mu = -sdT + \tau dP$	$\tau = \left. \frac{\partial \mu}{\partial P} \right\|_T ; s = -\left. \frac{\partial \mu}{\partial T} \right\|_P$
s	(τ,e)	$ds = \frac{P}{T}d\tau + \frac{1}{T}de$	$\frac{P}{T} = \left. \frac{\partial s}{\partial \tau} \right\|_e ; \frac{1}{T} = \left. \frac{\partial s}{\partial e} \right\|_\tau$
e	(τ,s)	$de = Tds - Pd\tau$	$P = -\left. \frac{\partial e}{\partial \tau} \right\|_s ; T = \left. \frac{\partial e}{\partial s} \right\|_\tau$

Table 1: Potentials defining a complete EOS in a given thermodynamical plane.

The stiffened gas (SG) EOS is often used, as in (39; 22), because of its simplicity and its analytical form enabling to easily change of thermodynamical plane. In the following, SG EOS will be used for water vapor v and non-condensable gas a (see section 2.1).

In (23), a more realistic EOS has been tested: it consists in a look-up table based on IAPWS-97 formulation (40), one industrial reference EOS dedicated to water. Here, we aim to propose a compromise between the simplicity of a SG and the numerical costs and difficulties of a IAPWS look-up table (see (23)), by choosing a semi-analytical EOS for the liquid l: a Noble-Able stiffened gas EOS (26; 28) modified with the Chemkin EOS (27), called NASG-CK EOS in the following (see section 2.2).

2.1 Stiffened gas EOS for the gaseous fields v and a

We recall the stiffened gas EOS in (τ, e)-plane for $k \in \{v, a\}$:

$$s_k(\tau_k, e_k) = C_{v,k} \ln \left((e_k - Q_k - \pi_k \tau_k) \tau_k^{\gamma_k - 1} \right) + s_{0k}. \tag{46}$$

The stiffened gas parameters are the following, for $k \in \{v, a\}$:

- $C_{v,k}$ $(J.K^{-1}.kg^{-1})$ is the calorific capacity at constant volume,
- γ_k is the adiabatic index, a non-dimensional coefficient greater than 1,
- $-\Pi_k$ (Pa) is the minimal admissible pressure (which can be negative),
- Q_k $(J.kg^{-1})$ is a reference enthalpy,
- s_{0k} $(J.K^{-1}.kg^{-1})$ is a reference entropy.

The coefficients, given in appendix 7, are evaluated with an optimization method, as described in chapter 2 of (37), based on a minimization of the relative errors (on chemical potential μ, specific volume τ and heat capacity C_p) between the SG EOS and IAPWS EOS on a large liquid domain.

This EOS can be explicitely written in (P,T)-plane using the definition $\mu = e - Ts + P\tau$:

$$\begin{aligned} &\forall k \in \{v,a\}, \\ &\mu_k(P_k,T_k) = \gamma_k C_{v,k} T_k + Q_k - T_k(\gamma_k C_{v,k} \ln(T_k) \\ &-(\gamma_k - 1) C_{v,k} \ln(P_k + \Pi_k) + k_k), \end{aligned} \tag{47}$$

with a constant k_k (in $J.K^{-1}.kg^{-1}$), defined in accordance with (46) and (49):

$$k_k = C_{v,k}(\ln(C_{v,k}) + (\gamma_k - 1)\ln(C_{v,k}(\gamma_k - 1))) + s_{0k}. \tag{48}$$

Other quantities can be deduced using table 1:

$$\begin{aligned} &\forall k \in \{v,a\}, \tau_k(P_k,T_k) = \frac{C_{v,k}(\gamma_k - 1)T_k}{P_k + \Pi_k}; \\ &s_k(P_k,T_k) = \gamma_k C_{v,k} \ln(T_k) \\ &-(\gamma_k - 1) C_{v,k} \ln(P_k + \Pi_k) + k_k; \\ &e_k(P_k,T_k) = C_{v,k} T_k + Q_k + C_{v,k}(\gamma_k - 1) T_k \frac{\Pi_k}{P_k + \Pi_k}; \\ &C_{p_k}(P_k,T_k) = C_{p_k} = \gamma_k C_{v,k}. \end{aligned} \tag{49}$$

Remark 4 — It can be easily checked that property 8 is verified for a SG EOS. However, as noted in remark 3, T might be negative if $z_k < 0$, which might happen with the stiffened gas EOS. Indeed, it can be proved from system (31) that $e_k - Q_k - \tau_k \Pi_k$, $(k = v, a)$, remains positive within time: in fact, some thermodynamical states might lead to an internal energy $e_k < 0$, depending on the chosen values for Q_k and Π_k. In our numerical tests, we observed such negative z_k only in very rare situations, when taking some $\lambda > 0$ leading to a too delayed return towards thermodynamical equilibrium.

2.2 Noble-Able-Chemkin stiffened gas EOS for the liquid l

In (28), the authors proved that Noble-Able Stiffened gas (NASG) EOS can be extended to cope with a variable heat capacity at constant pressure C_p (in $J.K^{-1}.kg^{-1}$) depending on the temperature: in particular, they recommend to define C_p with the NASA polynomials, used in the Chemkin EOS (27).

2.2.1 Definition in (P, T)-plane

Thus, we propose the following EOS, by gathering the main features of NASG EOS and Chemkin EOS i.e. the introduction of a specific volume $b_l > 0$ ($m^3.kg^{-1}$) and a variable C_{p_l} defined as a polynomial of T_l:

$$
\begin{aligned}
&\mu_l(P_l, T_l) = \mu_l^0(T_l) + b_l P_l + \mathcal{C}_l(T) \ln(P_l + \Pi_l), \\
&\text{with: } \mu_l^0(T_l) = RT_l \left(A_l(1 - \ln(T_l)) - \frac{B_l}{2} T_l \right. \\
&\left. - \frac{C_l}{6} T_l^2 - \frac{D_l}{12} T_l^3 - \frac{E_l}{20} T_l^4 + \frac{F_l}{T_l} - G_l \right), \\
&\mathcal{C}_l(T_l) = C_{v,l}(\gamma_l - 1) T_l, \\
&R = \frac{r}{M} \text{ the perfect gas constant,} \\
&\text{with } r = 8.31446261815324 \; J.kg^{-1}.mol^{-1} \\
&\text{and } M = 18.01528 \; g.mol^{-1}.
\end{aligned}
\tag{50}
$$

Other quantities can be deduced from (50) using table 1:

$$\begin{aligned}
&\tau_l(P_l,T_l) = b_l + \frac{C_{v,l}(\gamma_l-1)T_l}{P_l+\Pi_l};\\
&s_l(P_l,T_l) = R\left(A_l\ln(T_l) + B_lT_l + \frac{C_l}{2}T_l^2 + \frac{D_l}{3}T_l^3 + \frac{E}{4}T_l^4 + G_l\right)\\
&-C_{v,l}(\gamma-1)\ln(P_l+\Pi_l);\\
&C_{p_l}(T_l) = R(A_l + B_lT_l + C_lT_l^2 + D_lT_l^3 + E_lT_l^4);\\
&\alpha_{Pl}(P_l,T_l) = \frac{1}{\tau_l}\left.\frac{\partial^2\mu_l}{\partial P_l\partial T_l}\right|_{T_l,P_l} = \frac{C_v(\gamma-1)}{C_v(\gamma-1)T + b(P+\Pi)}.
\end{aligned} \tag{51}$$

2.2.2 *Definition in* (τ, e)*-plane*

Inverting the NASG-CK EOS from the (τ_l, e_l)-plane towards the (P_l, T_l)-plane requires an implicit resolution. Supposing that τ_l and e_l are known as functions of (P_l, T_l), we aim to get $s_l(\tau_l, e_l)$, using the two following equations:

$$P_l(T_l,\tau_l) = \frac{C_{v,l}(\gamma_l-1)T_l}{\tau_l-b_l} - \Pi_l = P_l(\tau_l,T_l); \tag{52}$$

$$\begin{aligned}
&e_l(T_l,\tau_l) = RT_l(A_l + \frac{B_l}{2}T_l + \frac{C_l}{3}T_l^2 + \frac{D_l}{4}T_l^3\\
&+\frac{E_l}{5}T_l^4 + \frac{F_l}{T_l}) - C_{v,l}(\gamma_l-1)T_l + \Pi_l(\tau_l-b_l).
\end{aligned} \tag{53}$$

More precisely:

1. T_l is obtained by implicitely solving equation (53), since e_l and τ_l are known;
2. P_l can then be explicitely computing from T_l and τ_l using equation (52).

At the end of day, we speak about "semi-analytical" EOS for NASG-CK because, up to an implicit resolution of $e_l(\tau_l, T_l)$ to find T_l, the complete EOS in (τ_l, e_l)-plane $s_l(\tau(P_l, T_l), e_l(\tau_l, T_l))$ can be obtained from $\mu_l(P_l, T_l)$.

2.2.3 *Admissibility condition of NASG-CK EOS*

Property 10

The Noble-Able Chemkin EOS (50) is an admissible EOS ensuring property 8 when:

$$C_{p_l}(T_l) - C_{v,l}(\gamma_l - 1) \geq 0 \tag{54}$$

It has been numerically checked that (54) holds for the coefficients used in this work (given in appendix 7).

Proof:

Here we focus on the concavity of $(\tau_l, e_l) \mapsto s_l(\tau_l, e_l)$ because all the other requirements from property 8 can be easily proved. Recalling from table 1:

$$\left.\frac{ds_l}{d\tau_l}\right|_{e_l} = \frac{P_l}{T_l} \quad ; \quad \left.\frac{ds_l}{de_l}\right|_{\tau_l} = \frac{1}{T_l},$$

one needs now to evaluate the second derivatives of $(\tau_l, e_l) \mapsto s_l(\tau_l, e_l)$. Using (53), we can deduce an implicit relation $T_l = T_l(\tau_l, e_l)$ and we get:

$$de_l = (C_{p_l}(T_l) - C_{v,l}(\gamma_l - 1))dT_l + \Pi_l d\tau_l, \tag{55}$$

so that:

$$\left.\frac{\partial T_l}{\partial \tau_l}\right|_{e_l} = -\Pi_l (C_{p_l}(T_l) - C_{v,l}(\gamma_l - 1))^{-1}, \tag{56}$$

and

$$\left.\frac{\partial T_l}{\partial e_l}\right|_{\tau_l} = (C_{p_l}(T_l) - C_{v,l}(\gamma_l - 1))^{-1}. \tag{57}$$

Moreover, using (52), we get also:

$$P_l = \frac{C_{v,l}(\gamma_l - 1)T_l(\tau_l, e_l)}{\tau_l - b_l} - \Pi_l, \tag{58}$$

so that:

$$\left.\frac{\partial P_l}{\partial \tau_l}\right|_{e_l} = -\frac{C_{v,l}(\gamma_l - 1)T_l}{(\tau_l - b_l)^2} + \frac{C_{v,l}(\gamma_l - 1)}{(\tau_l - b_l)} \left.\frac{\partial T_l}{\partial \tau_l}\right|_{e_l}. \tag{59}$$

It reads then:

$$\begin{aligned}\frac{\partial^2 s_l}{\partial \tau_l \partial e_l} &= \frac{\partial}{\partial \tau_l}\left(\frac{1}{T_l}\right)\Big|_{e_l} = -\frac{1}{T_l^2}\frac{\partial T_l}{\partial \tau_l}\Big|_{e_l} \\ &= \frac{\Pi_l}{T_l^2}(C_{p_l}(T_l) - C_{v,l}(\gamma_l - 1))^{-1};\end{aligned} \tag{60}$$

$$\begin{aligned}\frac{\partial^2 s_l}{\partial e_l^2}\Big|_{\tau_l} &= \frac{\partial}{\partial e_l}\left(\frac{1}{T_l}\right)\Big|_{\tau_l} = -\frac{1}{T_l^2}\frac{\partial T_l}{\partial e_l}\Big|_{\tau_l} \\ &= -\frac{1}{T_l^2}\left(C_{p_l}(T_l) - C_{v,l}(\gamma_l - 1)\right)^{-1};\end{aligned} \tag{61}$$

$$\begin{aligned}&\frac{\partial^2 s_l}{\partial \tau_l^2}\Big|_{e_l} = \frac{\partial}{\partial \tau_l}\left(\frac{P_l}{T_l}\right)\Big|_{\tau_l} = \frac{1}{T_l}\frac{\partial P_l}{\partial \tau_l}\Big|_{e_l} - \frac{P_l}{T_l^2}\frac{\partial T_l}{\partial \tau_l}\Big|_{e_l} \\ &= \frac{\partial T_l}{\partial \tau_l}\Big|_{e_l}\left(\frac{C_{v,l}(\gamma_l - 1)}{T_l(\tau_l - b_l)} - \left(\frac{C_{v,l}(\gamma_l - 1)}{T_l(\tau_l - b_l)} - \frac{\Pi_l}{T_l^2}\right)\right) \\ &- \frac{C_{v,l}(\gamma_l - 1)}{(\tau_l - b_l)^2} \\ &= -\frac{\Pi_l^2}{T_l^2}(C_{p_l}(T_l) - C_{v,l}(\gamma_l - 1))^{-1} - \frac{C_{v,l}(\gamma_l - 1)}{(\tau_l - b_l)^2} \\ &= -\Pi_l \frac{\partial^2 s_l}{\partial \tau_l \partial e_l} - \frac{C_{v,l}(\gamma_l - 1)}{(\tau_l - b_l)^2}.\end{aligned} \tag{62}$$

Since $C_{p_l}(T_l) - C_{v,l}(\gamma_l - 1) \geq 0$, we get:

$$\begin{aligned}&\frac{\partial^2 s_l}{\partial \tau_l^2}\Big|_{e_l} \leq 0 \quad ; \quad \frac{\partial^2 s_l}{\partial e_l^2}\Big|_{\tau_l} \leq 0 \\ &\frac{\partial^2 s_l}{\partial \tau_l^2}\Big|_{e_l}\frac{\partial^2 s_l}{\partial e_l^2}\Big|_{\tau_l} - \left(\frac{\partial^2 s_l}{\partial \tau_l \partial e_l}\right)^2 \\ &= \left(\frac{\partial^2 s_l}{\partial \tau_l \partial e_l}\right)^2 (1 - 1) + \frac{\partial^2 s_l}{\partial \tau_l \partial e_l}\frac{C_{v,l}(\gamma_l - 1)}{(\tau_l - b_l)^2 \Pi_l} \\ &= \frac{C_{v,l}(\gamma_l - 1)}{(\tau_l - b_l)^2 T_l^2}\left(C_{p_l}(T_l) - C_{v,l}(\gamma_l - 1)\right)^{-1} \geq 0,\end{aligned} \tag{63}$$

which proves that $(\tau_l, e_l) \mapsto s_l(\tau_l, e_l)$ is indeed concave as required by property 8.

2.2.4 Evaluation of NASG-CK EOS coefficients

The procedure is the following:

- EOS coefficients A_l, B_l, C_l, D_l and E_l have been evaluated by fitting the specific volume τ_l and the heat capacity $C_{p,l}$ to data obtained with IAPWS EOS (see chapter 2 of (37)).

- γ_l, $C_{v,l}$, Π_l and b_l have been defined by extending the empirical method proposed in (41) for the stiffened gas EOS, by imposing the specific volume $\tau_l(P_0, P_0)$, the thermal expansion coefficient $\alpha_{P,l}(P_0, T_0)$, the specific heat capacity at constant volume $C_{v,l}(P_0, T_0)$ as well as the sound speed $c_l(P_0, T_0)$ at a reference point (P_0, T_0) (see appendix 11).

- The remaining coefficients F_l and G_l have been defined by fitting $(\mu_l - \mu_v)(T^{sat}_{IAPWS}(P))$ to zero (see appendix 11).

Resulting coefficients are given in appendix 7.

2.2.5 *Accuracy of NASG-CK EOS*

We compared NASG-CK EOS with a liquid SG EOS, obtained with the minimization procedure from (37). All EOS coefficients are given in appendix 7. Recalling the definition of the relative error err_ϕ for a quantity ϕ:

$$err_\phi = \left| \frac{\phi^{EOS} - \phi^{IAPWS}}{\phi^{IAPWS}} \right|,$$

we chose the following (subjective) indicators, gathered in table 2:

- the mean, minimal and maximal relative error for each quantity;

- the percentage of the physical domain in (P, T)-plane where the relative error is smaller than 5% for each quantity;

- the percentage of the physical domain in (P, T)-plane where the relative error is smaller than 5% for the three quantities τ and C_p at the same time;

Error maps for τ_l (figures 1 and 2) and C_{p_l} (figures 3 and 4) are also given, showing the relative error at each point (P_l, T_l), with an error limited by a ceiling of 5%.

All the previous indicators show that NASG-CK EOS is far more accurate than a SG EOS on a large liquid domain.

Indicators (%)		NASG CK EOS	SG EOS
Mean relative errors	on τ	3.0	9.6
	on C_p	0.87	7.0
Min relative errors	on τ	$\simeq 10^{-6}$	$\simeq 10^{-7}$
	on C_p	$\simeq 10^{-6}$	$\simeq 10^{-6}$
Max relative errors	on τ	20	29
	on C_p	22	55
% of domain with err $< 5\%$	on τ	78	26
	on C_p	99	33
	on τ and C_p	78	13

Table 2: Comparison of accuracy indicators for NASGCK EOS and SG on a large liquid domain, relatively to IAPWS

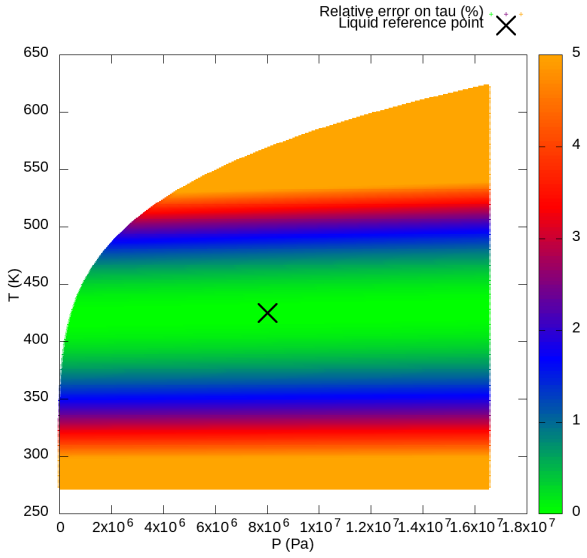

Figure 1: Relative error on τ compared with IAPWS-97 for NASGCK EOS, with error saturation at 5%.

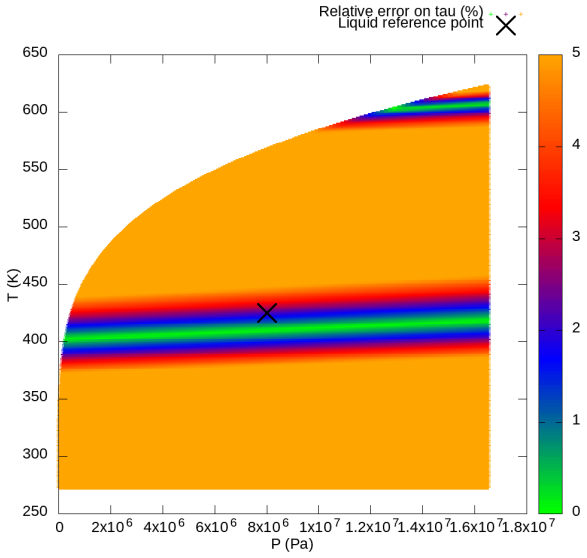

Figure 2: Relative error on τ compared with IAPWS-97 for SG EOS, with error saturation at 5%.

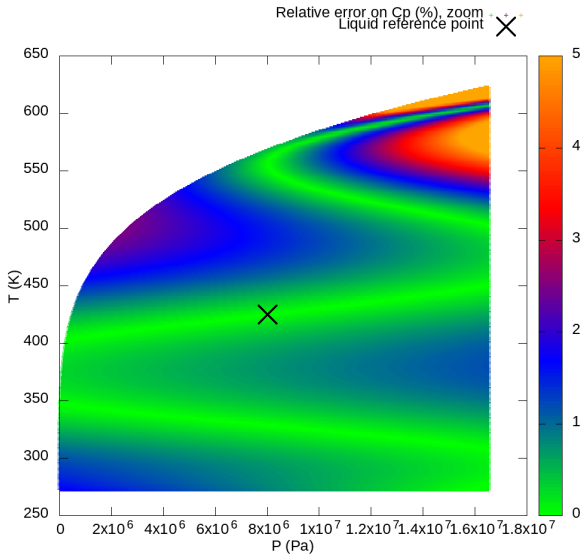

Figure 3: Relative error on C_p compared with IAPWS-97 for NASGCK EOS, with error saturation at 5%.

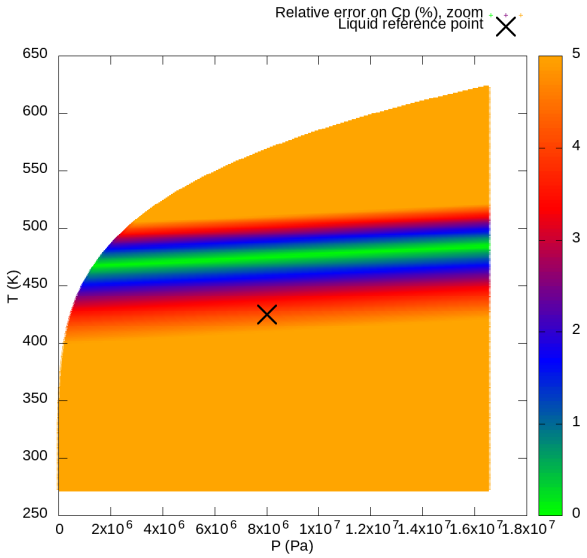

Figure 4: Relative error on C_p compared with IAPWS-97 for SG EOS, with error saturation at 5%.

3 Numerical implementation

The numerical implementation is carried out following the same numerical strategy as in (22; 23). We will only recall here the main features of the method and we refer to the previous references for more details. The numerical method is based on a fractional step method (42) using a Lie-Trotter splitting (with a unique sub-iteration). More precisely, system of equations (31) can be rewritten as:

$$\frac{\partial W}{\partial t} = -\frac{\partial \mathcal{F}(W)}{\partial x} + \mathcal{G}(W), \quad W(t=0) = W^0, \tag{64}$$

where $\mathcal{F}$ correspond to the convective flux and $\mathcal{G}$ to the source terms. A straightforward Lie-Trotter splitting is chosen, consisting in solving at time $t = t^n$ the following two sub-systems during a time step Δt^n:

$$(i) \quad \frac{\partial W_a}{\partial t} = -\frac{\partial \mathcal{F}(W_a)}{\partial x}, \quad W_a(t^n) = W^n, \tag{65}$$

which gives $W_a(t^n + \Delta t^n)$. Then, for the second step, the following equations are solved:

$$(ii) \quad \frac{\partial W_b}{\partial t} = G(W_b), \quad W_b(t = t^n) = W_a(t^n + \Delta t^n), \tag{66}$$

which gives $W^{n+1} = W_b(t^n + \Delta t^n)$. Since this splitting is first order with respect to time, each sub-system is solved using first order schemes.

3.1 Numerical schemes to solve the convective sub-system (65)

First sub-system (65) takes into account the convective part: it is solved with first-order explicit and conservative finite volumes schemes. Their general form for a one-dimensional framework with cells Ω_i is:

$$\begin{aligned} &|\Omega_i|(W_i^{n+1} - W_i^n) = \\ &-\Delta t^n((F(W_i^n, W_{i+1}^n) - F(W_{i-1}^n, W_i^n)), \end{aligned} \tag{67}$$

where W_i^n denotes the space-average value of W on the cell Ω_i at time t^n. Note that other methods may be used, as in (29) where a similar model has been implemented using a Lattice-Boltzmann method. In this work, two different schemes are used: Rusanov

scheme (43) and a relaxation scheme proposed in (44) and used in (23) for complex EOS. We recall very briefly their main features and we refer to previous references for more details.

For the Rusanov scheme, the numerical flux is:

$$\begin{aligned} F(W_l, W_r) &= \frac{1}{2}(\mathcal{F}(W_l) + \mathcal{F}(W_r)) - \\ &\quad \frac{\max(\Lambda_r, \Lambda_l)}{2}(W_r - W_l), \end{aligned} \tag{68}$$

where Λ_r (resp. Λ_l) is the spectral radius of the convection matrix $\nabla_W \mathcal{F}$ at $W = W_r$ (resp. $W = W_l$). The time step Δt^n at iteration n should satisfy the CFL constraint:

$$\frac{\Delta t^n}{\Delta x} \max(\Lambda_r, \Lambda_l) < \frac{1}{2}. \tag{69}$$

As far as the relaxation scheme is concerned, an enlarged hyperbolic system is introduced, associated with a strong relaxation term, so that the relaxation procedure enables to formally recover the initial system of equations. The enlarged system to solve is then the following:

$$\begin{cases} \partial_t(\rho Y) + \partial_x(\rho Y U) = 0; \\ \partial_t \rho + \partial_x(\rho U) = 0; \\ \partial_t(\rho U) + \partial_x(\rho U^2 + \Pi) = 0; \\ \partial_t(\rho \Sigma) + \partial_x(\rho U \Sigma + U \Pi) = 0; \\ \partial_t(\rho \mathcal{T}) + \partial_x(\rho \mathcal{T} U) = \frac{1}{\epsilon}\rho(\tau - \mathcal{T}); \end{cases} \tag{70}$$

where the relaxation source terms for $\mathcal{T}$ are characterized by the parameter $\epsilon \geq 0$. Some additional variables have been introduced to build system (70): one additional scalar unknown $\mathcal{T}$ with the initial condition:

$$\forall x,\ \mathcal{T}(0, x) = \tau(0, x);$$

a relaxed pressure Π:

$$\Pi = P(Y, \mathcal{T}, e) + a^2(\mathcal{T} - \tau); \tag{71}$$

and a relaxed specific total energy Σ:

$$\Sigma = \frac{u^2}{2} + e + \frac{\Pi^2 - P^2(Y, \mathcal{T}, e)}{2a^2}, \tag{72}$$

as well as a positive parameter a, which should satisfy the following sub-characteristic condition:

$$a > \max\left(\frac{c_l(Y_l, \tau_l, e_l)}{\tau_l}, \frac{c_r(Y_r, \tau_r, e_r)}{\tau_r}\right). \tag{73}$$

The numerical flux is the following:

$$F(W_l, W_r) = \left(\frac{YU}{\tau}, \frac{U}{\tau}, \frac{U^2}{\tau} + \Pi, \frac{U\Sigma}{\tau} + U\Pi\right),$$

where Y, τ, U, Σ are the components of $\mathcal{Z}\,(x/t = 0, Z_l, Z_r)$, the self-similar solution $\mathcal{Z}\,(x/t, Z_l, Z_r)$ of the Riemann problem associated with the homogeneous part of (70) at the interface separating cells l and r, so that Π=$\Pi(Y, \tau, \Sigma)$. In practice, we use the relaxation scheme by enforcing $\epsilon \to 0$.

3.2 *Applying the source terms through sub-system* (66)

The return towards thermodynamical equilibrium is accounted for with second subsystem (66), which reads:

$$\begin{cases} \dfrac{\partial}{\partial t}(Y) = \dfrac{\bar{Y}(\tau, e) - Y}{\lambda(t)}; \\ \dfrac{\partial}{\partial t}(\rho) = 0; \\ \dfrac{\partial}{\partial t}(\rho U) = 0; \\ \dfrac{\partial}{\partial t}(\rho E) = 0. \end{cases} \tag{74}$$

In this second subsystem (74), τ and e are constant:

$$\tau(t) = \tau(0) \quad ; e(t) = e(0).$$

We make furthermore the approximation: $\lambda(t) = \lambda(0)$, so that the fractions can be computed as the exact solutions of the approximated sub-system:

$$\frac{\partial Y}{\partial t} = \frac{\bar{Y}(\tau(0), e(0)) - Y}{\lambda(0)}. \tag{75}$$

For an initial condition given by the value at time t^n, the final approximation at time $t^{n+1} = t^n + \Delta t^n$ then reads:

$$\begin{cases} Y(t^{n+1}) = Y(t^n)\, e^{\frac{-\Delta t^n}{\lambda(t^n)}} + \bar{Y}(t^n)\, \left(1 - e^{\frac{-\Delta t^n}{\lambda(t^n)}}\right); \\ \rho(t^{n+1}) = \rho(t^n); \\ U(t^{n+1}) = U(t^n); \\ e(t^{n+1}) = e(t^n). \end{cases} \tag{76}$$

Remark 5 — For the sake of simplicity, both sub-systems (65) and (66) are solved using only one time-step. Since the explicit numerical scheme of the convective sub-system imposes a stability constraint on this time-step, this second step is achieved using an implicit scheme.

The major difficulty in this step is in fact to compute the thermodynamical equilibrium $\bar{Y}$: the algorithm, based on (14), is briefly explained in the next section 3.3 and fully described in appendix 9.

3.3 Principles enabling to compute the thermodynamical equilibrium

After the convection step, (y_a, τ, e) are known and we need now to find the equilibrium fractions $\bar{Y}(y_a, \tau, e) = (\bar{\alpha}_v, \bar{y}_v, \bar{z}_v, y_a)$ enabling to maximize the mixture entropy s (36) for a fixed (τ, e, y_a). The main procedure is the following:

ALGORITHM 1 (Type of equilibrium) — Arguments: (y_a, τ, e).

- **If y_a = 1**: the equilibrium is a monophasic state with only field a, so that:

$$\bar{\alpha}_v = 0 \quad ; \quad \bar{y}_v = 0 \quad ; \quad \bar{z}_v = 0 \quad ; \quad \bar{z}_a = 1.$$

- **Else if y_a = 0**: we compute an equilibrium state with the two fields l and v using ALGORITHM 2 (LV), computing a potential equilibrium $\bar{Y}^{lv}(y_a, \tau, e) = (\tilde{\alpha}_v^{lv}, \tilde{y}_v^{lv}, \tilde{z}_v^{lv}, \tilde{z}_a^{lv})$.

- **If $\bar{Y}^{lv}$ is admissible** (i.e. if all the fractions are in $]0,1[$):

$$\bar{Y} = \bar{Y}^{lv}.$$

- **Else**: the equilibrium state is a monophasic state with only l or only v. More precisely, the equilibrium state is the monophasic state maximizing the entropy:

  * **If** $s_l(\tau, e) > s_v(\tau, e)$: the equilibrium is a pure liquid water state, so that:

$$\bar{\alpha}_v = 0 \quad ; \quad \bar{y}_v = 0 \quad ; \quad \bar{z}_v = 0 \quad ; \quad \bar{z}_a = 0.$$

  * **Else**: the equilibrium is a pure water vapor state, so that:

$$\bar{\alpha}_v = 1 \quad ; \quad \bar{y}_v = 1 \quad ; \quad \bar{z}_v = 1 \quad ; \quad \bar{z}_a = 0.$$

- **Else**: we compute an equilibrium state $\tilde{Y}^{lva}(y_a, \tau, e)$ with the three fields l, v and a, determined using ALGORITHM 3 (LVA):

  - **If $\bar{Y}^{lva}$ is admissible** (i.e. if all the fractions are in $]0,1[$):

$$\bar{Y} = \tilde{Y}^{lva}.$$

  - **Else**: the equilibrium state is a mixture of l and a, or a mixture of v and a. Both possible states $\tilde{Y}^{la}(y_a, \tau, e)$ and $\tilde{Y}^{va}(y_a, \tau, e)$ are computed using ALGORITHM 4 (LA) and ALGORITHM 5 (VA), thanks to conditions from property 4. The physical state is obtained by comparing both mixture entropies $s_{ka} = (1 - y_a)s_k(\tilde{\tau}_k, \tilde{e}_k) + y_a s_a(\tilde{\tau}_a, \tilde{e}_a)$, $k = l, v$:

    * **If** $s_{la}(y_a, \tau, e) > s_{va}(y_a, \tau, e)$: the equilibrium is a two-phase mixture of liquid water and non-condensable gas, so that

$$\bar{Y} = \bar{Y}^{la}.$$

    * **Else**: the equilibrium is a miscible gaseous mixture of water vapor and non-condensable gas, so that:

$$\bar{Y} = \bar{Y}^{va}.$$

The previous procedure calls algorithms to compute the thermodynamical equilibrium, depending on the fields which are actually present in the mixture. These algorithms are described in details in appendix 9. The LV-equilibrium (ALGORITHM 2) and the LVA-equilibrium (ALGORITHM 3) algorithms are based on the algorithm initially proposed in (14). The key idea is to use a change of thermodynamical plane. Indeed, if we consider the LVA-case, the equilibrium is characterized by the four following equations in the (τ, e)-plane:

$$\begin{aligned}
&P_l(\tau_l, e_l) = P_v(\tau_v, e_v) + P_a(\tau_a, e_a);\\
&T_l(\tau_l, e_l) = T_v(\tau_v, e_v);\\
&T_v(\tau_v, e_v) = T_a(\tau_a, e_a);\\
&\mu_l(P_l(\tau_l, e_l), T_l(\tau_l, e_l)) = \mu_v(P_v(\tau_v, e_v), T_v(\tau_v, e_v));
\end{aligned} \tag{77}$$

since the previous system can be rewritten using relations $\tau_k = \dfrac{\alpha_k}{y_k}\tau$ and $e_k = \dfrac{z_k}{y_k}e$ for $k = l, v, a$: the four remaining unknowns are thus the equilibrium fractions, noted $\bar{\alpha}_v$, $\bar{y}_v$, $\bar{z}_v$ and $\bar{z}_a$. Instead of looking for these fractions $\bar{\alpha}_v$, $\bar{y}_v$, $\bar{z}_v$ and $\bar{z}_a$ satisfying (77), the idea, proposed in (14) and used for instance in (**?** 23), is to rather consider the following unknowns $\bar{P}_v$, $\bar{P}_a$, $\bar{T}$ and $\bar{y}_v$. Miscibility constraints (7) enable to get a system equivalent to system (77) in the pressure-temperature plane:

$$\begin{aligned}
&\bar{y}_v \times \tau_v(\bar{P}_v, \bar{T}) = y_a \times \tau_a(\bar{P}_a, \bar{T});\\
&\tau = (1 - \bar{y}_v) \times \tau_l(\bar{P}_v + \bar{P}_a, \bar{T}) + \bar{y}_v \times \tau_v(\bar{P}_v, \bar{T});\\
&e = (1 - \bar{y}_v) \times e_l(\bar{P}_v + \bar{P}_a, \bar{T}) + \bar{y}_v \times e_v(\bar{P}_v, \bar{T})\\
&+ y_a \times e_a(\bar{P}_a, \bar{T});\\
&\mu_l(\bar{P}_v + \bar{P}_a, \bar{T}) = \mu_v(\bar{P}_v, \bar{T}).
\end{aligned} \tag{78}$$

With the particular choice for phasic EOS considered in section 2, system (78) can be rewritten as a system of the coupled equations of only two variables ($\bar{P}_v$ and $\bar{P}_a$), corresponding to the second and the third equations of (78), solved in ALGORITHM 3 with a Broyden algorithm, as described in appendix 9.

Remark 6 (Analytical phasic EOS for v and a) — Without specifying any phasic EOS, the only obvious simplification of system (78) is to replace $\bar{y}_v$ by its expression as a function of $\bar{P}_v$, $\bar{P}_a$ and $\bar{T}$ obtained from the first equation of (78):

$$\bar{y}_v = y_a \frac{\tau_a(\bar{P}_a, \bar{T})}{\tau_v(\bar{P}_v, \bar{T})}.$$

It remains a system of three coupled equations of three unknowns $\bar{P}_v$, $\bar{P}_a$ and $\bar{T}$. Our particular choice of stiffened gas EOS for the vapor and the non-condensable gas enables to get an explicit formula for $\bar{T}$ as a function of $\bar{P}_v$ and $\bar{P}_a$. This is no longer the case when replacing the SG phasic EOS for vapor by a Noble-Able equation (26).

Remark 7 (Threshold for fractions) — In practice, a threshold $\epsilon_{frac} = 10^{-12}$ is defined in the code for the fractions: a fraction $1 \geq \varphi > 1 - \epsilon_{frac}$ will be taken equal to 1 and a fraction $0 \leq \varphi < \epsilon_{frac}$ will be taken equal to 0.

4 Verification test cases

In order to verify the implementation of the numerical methods as well as the thermodynamical equilibrium computation, convergence studies are performed on Riemann problems for which a unique analytical solution can be exhibited.

As in (23; 39), particular Riemann problems with only a contact wave and a shock wave are built. More precisely, we consider a one-dimensional domain $x \in [0\ m, 1\ m]$, discretized using uniform meshes, with an initial discontinuity at $x_d = 0.5\ m$. The exact solution (see figure 5) consists in the left and right initial states, respectively W^L and W^R, separated by a uniform intermediate state W^*. The nature of waves is the following:

- the wave travelling at $U - c$ is a ghost wave;

- the wave travelling at U, separating left state W^L and intermediate state W^*, is a contact-wave;
- the wave travelling at $U + c$, separating intermediate state W^* and right state W^R, is a shock-wave.

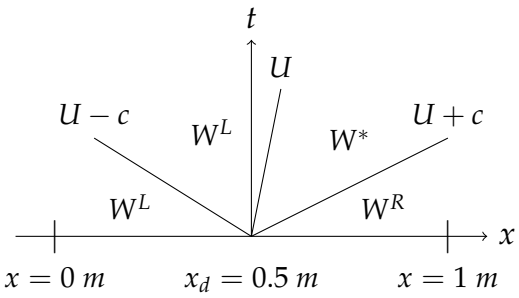

Figure 5: Riemann problem with one intermediate state; U-c: ghost wave; U: contact wave; U+c: shock wave

As in (23), two types of Riemann problems are considered:

- "out-of-equilibrium" Riemann problems, with $\lambda \to \infty$: only the convective part of model 1 is tested;
- "at-equilibrium" Riemann problem, with $\lambda \to 0$: first, the convective terms are taken into account and the thermodynamical equilibrium is then enforced through the source terms, as depicted in section 3.3.

Computing the analytical solutions is classical but somehow tricky because of the non-condensable gas: the method is presented in the next section. Then, convergence results for out-of-equilibrium Riemann problems (section 4.2) and for at-equilibrium Riemann problems (section 4.3) are presented. The initial data for each test case are reported in appendix 8. Convergence studies are performed by computing the relative L^1-error, defined

as follows: for an approximated solution Ψ^{approx} and an exact solution Ψ^{exact}, since the mesh size is uniform, the relative L^1-error is computed at time t^n on the whole mesh as:

$$\frac{\sum_i |\Psi_i^{approx,n} - \Psi^{exact}(x_i, t^n)|}{\sum_i |\Psi^{exact}(x_i, t^n)|},$$

where x_i is the barycenter of the cell i. Obviously, when $\sum_i |\Psi^{exact}(x_i, t^n)| = 0$ (i.e. $\Psi^{exact} = 0$), this relative error is meaningless and we then consider the mere L^1-error:

$$\sum_i |\Psi_i^{approx,n} - \Psi^{exact}(x_i, t^n)|.$$

4.1 General method to build analytical solutions

The main approach is the same as the one used in (45; 22; 23). First a left state W^L is chosen; then the intermediate state W^* is computed across the contact wave from W^L thanks to conditions (44); last, the right state W^R is obtained from W^* through the shock wave thanks to conditions (43).

For a **out-of-equilibrium Riemann problem**, P is the mixture pressure from (38), so that $P = P(Y, \tau, e)$, directly evaluated with the variables Y, τ, e computed through the convection step (65).

For an **at-equilibrium Riemann problem**, P is always computed with (38), but no more with the convected fractions Y: this time, $P = P(\bar{Y}, \tau, e) = \bar{P}$, with $\bar{Y} = \bar{Y}(\tau, e)$ the equilibrium fractions computed with algorithms from appendix 9. We highlight that, for Riemann problems at equilibrium, **only the mass fraction y_a is convected** and still complies with $J[y_a] = 0$: the other equilibrium fractions $\bar{\alpha}_v$, $\bar{y}_v$, $\bar{z}_v$ and $\bar{z}_a$ do not verify the jump relations anymore.

The detailed algorithms enabling to build such Riemann problems are given in appendix 10.

4.2 *Out-of-equilibrium test cases*

An out-of-equilibrium Riemann problem is considered in table 8.1 in appendix, where the data is obtained using out-of-equilibrium problem algorithm from appendix 10. The expected convergence rate of $\frac{1}{2}$, due to the presence of the contact wave, is observed on the convergence curves (see figure 6).

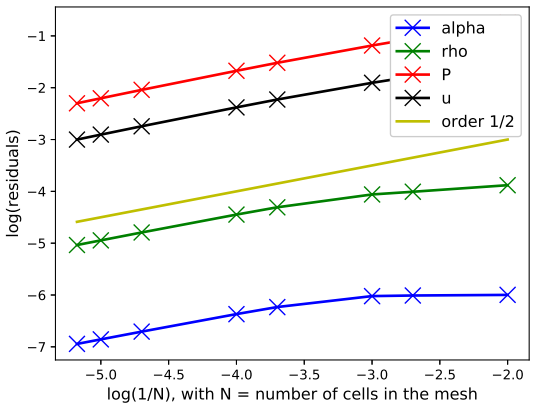

Figure 6: Convergence curve for Riemann problem 1 (out-of-equilibrium): meshes from 100 to 150 000 cells

4.3 *At-equilibrium test cases*

Two at-equilibrium Riemann problems are considered, obtained by using at-equilibrium problem algorithm from appendix 10:

- a first Riemann problem, with an initial pressure gap around 10 bar (see initial data in table 8.2 in appendix);
- a more brutal Riemann problem, with an initial pressure gap around 150 bar, in order to prepare the validation case SUPERCANON of section 5 (see initial data in table 8.3 in appendix).

In both cases, the asymptotical convergence rate is between $\frac{1}{2}$ and 1, as expected (see figures 7 and 8). A higher initial pressure gap seems to induce a slightly higher error on the pressure, but not really on the other quantities.

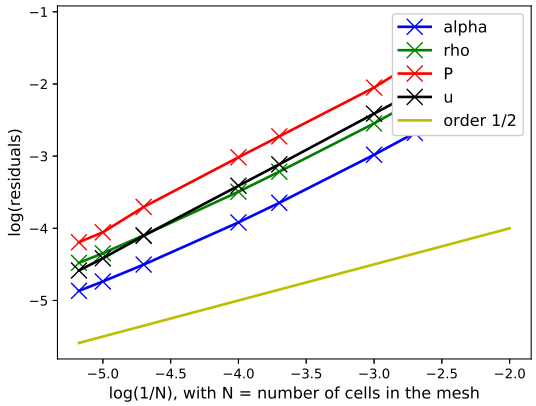

Figure 7: Convergence curve for Riemann problem 2 (at-equilibrium, with a $\simeq$ 10 bar pressure gap): meshes from 100 to 150 000 cells

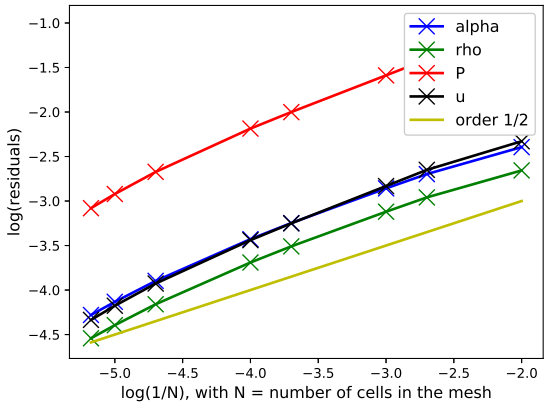

Figure 8: Convergence curve for Riemann problem 3 (at-equilibrium, with a $\simeq$ 150 bar pressure gap): meshes from 100 to 150 000 cells

5 Validation test case: SUPERCANON simulations

A validation test case is now considered, based on the SUPERCANON experiment (46), aiming at reproducing a simplified loss of coolant accident (LOCA) scenario. The experimental set-up is described on figure 9. A tube is filled with pressurized liquid water at 150 bar and 300°C (in order to be representative of the primary circuit of a pressurized water reactor). At the beginning of the experiment, the cap is removed, so that

the liquid water is now at the contact of the ambiant air at 1 bar and 20°C.

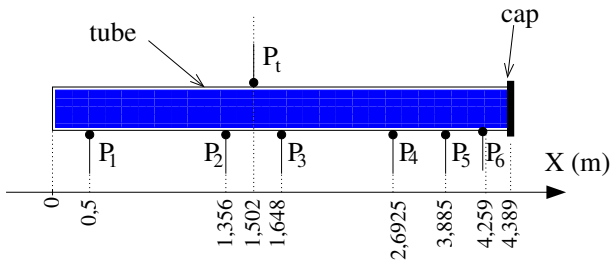

Figure 9: SUPERCANON experimental set-up (46)

A rough description of the main phenomena occuring during a SUPERCANON run is the following: the initial pressure gap creates a fast depressurization wave, which travels in the tube to the left. The pressure drops to a pressure around the saturation pressure, leading to the vaporisation of a small amount of liquid. The vapor fraction then increases slowly and the pressure remains almost constant until the arrival of the vaporisation front. This vaporisation front, which travels from the opening of the tube to the end of the tube, produces smoother changes of the pressure. It is responsible for the last pressure drop. Figure 10 shows the pressure evolution within time, measured at point P1 (see figure 9). Due to the importance of the initial pressure gap (around 150 bar), the observed pressure plateau does not match with the expected pressure saturation. It appears that the flow remains out of the thermodynamical equilibrium for a moment within a run, in particular close to the wall when the depressurization wave reaches the end of the tube. Previous numerical works (22; 47) based on a similar homogeneous model as the one studied here (18) highlight that taking into account the out-of-equilibrium effects is essential to obtain qualitatively correct results.

In the following, SUPERCANON simulations are performed on a mesh containing 2000 cells, on a domain of 10 meters, including the tube with a length of 4.389 m in its left part. The present work aims to better assess the importance of several parameters:

- the initial air mass fraction dissolved in liquid water. Liquid water has been degased

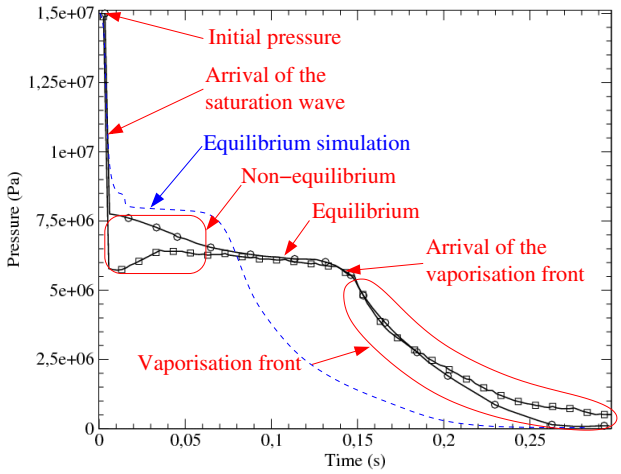

Figure 10: Pressure at P_1 (see Figure 9) within time

in SUPERCANON experiment, but the residual air fraction, even if it is very small, may have a strong influence on the simulations, as it has been highlighted in similar simulations (3);

- the relaxation time scale λ, defined in hypothesis 7. Some toy laws have been used in (22; 47), leading to a rather good agreement with the experimental results. These laws are here compared with a simplified model based on the nucleation theory, proposed in (23).

5.1 At-equilibrium simulations

Simulations are performed by taking $\lambda = 0$ and by chosing several y_a in the tube (see table 3). Results can be seen on figure 11. When the air mass fraction is very small (cases $y_a = 0$, $y_a = 10^{-6}$, $y_a = 5 \times 10^{-6}$, $y_a = 5 \times 10^{-5}$, $y_a = 10^{-4}$), the pressure suddently decreases and is then almost constant for a while. The pressure plateau on point P1 is overestimated, as expected because of the thermodynamical equilibrium assumption (see figure 11a). The more air there is, the smoother is the pressure drop. When the air mass fraction is quite important (cases $y_a = 10^{-2}$, $y_a = 10^{-3}$), the pressure drop is even delayed and becomes so smooth that the plateau is no longer observed. For cases $y_a = 0$, $y_a = 10^{-6}$, $y_a = 5 \times 10^{-6}$, the slightly different initial air mass fraction leads to slight

differences in the very first milliseconds of the experiment (see figure 11b).

In pure liquid, the depressurization at point P_1 (see figure 9) appears too early comparing with the experiment (around $\simeq 0.003s$ instead of $\simeq 0.004s$; see figure 11b). The sound speed is thus overestimated in our simulation. On one hand, thanks to experimental data, the experimental sound speed can be estimated around $\simeq 900m.^{-1}$. On the other hand, we compared the sound speed computed with NASG-CK EOS and obtained with IAPWS closed to the reference point $(P_0 = 80bar, T_0 = 425K)$, chosen to fit NASG-CK parameter (see appendix 11): NASG-CK sound speed is quite stable around $\simeq 1480m.s^{-1}$, which is the correct order of magnitude obtained with IAPWS-IF97 around (P_0, T_0). This observation incites to consider that a small amount of air is in fact dissolved in the liquid water: indeed, by choosing $y_a = 5 \times 10^{-5}$, the depressurization wave has this time a velocity in accordance with the experimental data (see figure 11b).

	Left State	**Right State**
Components of the mixture	Liquid water + Air	Air + Vapor (moist rate=55 %)
y_a ?	various y_a	$y_a = 0.0085162$
Pressure (Pa)	150 bar	1 bar
Temperature (°C)	300 °C	20 °C

Table 3: Initialization of the simulations: quantity of air for both left and right states.

5.2 Out-of-equilibrium simulations

5.2.1 Time scale following a "toy" law

First results have been obtained by using a toy law for λ, improved from (22) and also used in (47). The law is the following:

$$\lambda = t_{toy} = \lambda_0 \, f(\alpha_v) \, e^{-\left(\frac{|\alpha_v - \bar{\alpha}_v|}{\delta\alpha}\right)^2}, \tag{79}$$

where the function $\alpha \in [0,1] \mapsto f(\alpha)$ corresponds to 3 constant values with cosine connections to get a smooth function, as defined on figure 12. The law used to compute the

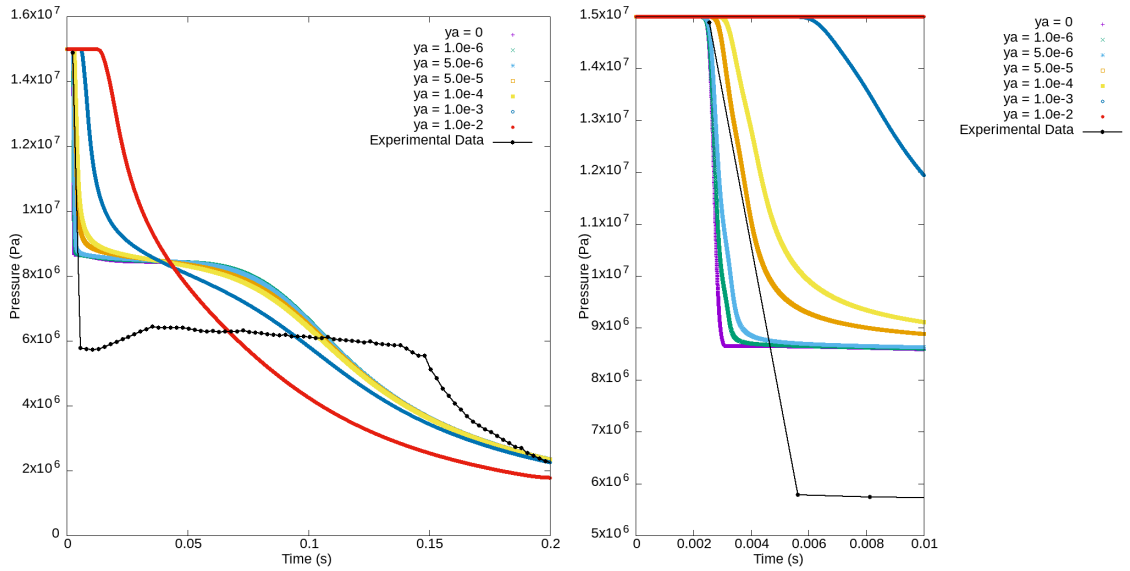

(a) Comparison between simulations and experimental data.

(b) Zoom on the first miliseconds: differences arise, depending on y_a.

Figure 11: Pressure (Pa) within time (s) at point P1 (see figure 9): at-equilibrium simulation ($\lambda = 0$), using NASG-CK EOS for the liquid with several initial air fractions y_a.

results presented below has the following parameters : $\lambda_0 = 1.5\ 10^{-2}\ s$ et $\delta\alpha = 5.5\ 10^{-4}$, $a = 1$, $b = 0.05$, $c = 0$, $\alpha_1 = 0$, $\alpha_2 = 0.15$, $\alpha_3 = 0.25$, $\alpha_4 = 0.65$.

5.2.2 *Time scale following a simplified model based on nucleation theory*

Some tests have been made using for λ a simplified model t_{nuc} based on nucleation theory, proposed in (23), from assumptions made for instance in (48) or (49). It reads:

$$\boxed{t_{nuc} = \left(\frac{a_0}{\Delta P}\right)^3 \exp\left(\frac{\varphi E_a}{k_B T}\right)}, \tag{80}$$

where E_a is defined from $\Delta P = |P_l - P_{sat}|$ and γ, the surface tension estimated from the IAPWS 94 correlation (50):

$$E_a = \frac{16\pi\gamma^3}{3(\Delta P)^2}, \tag{81}$$

and

$$\gamma = B_0(1 + b(1 - \frac{T}{T_c}))\left(\frac{T}{T_c}\right)^{\nu}, \tag{82}$$

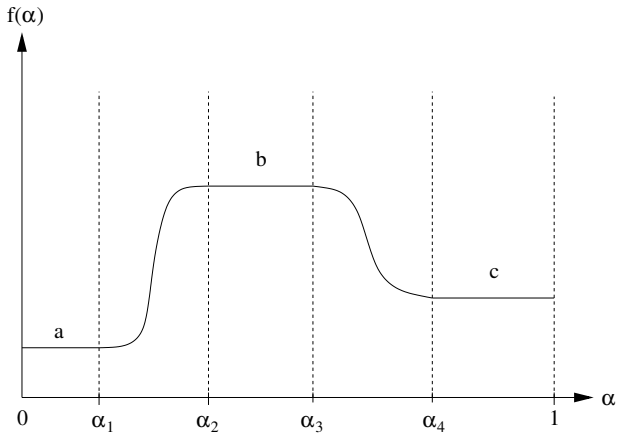

Figure 12: Definition of the function $\alpha \in [0,1] \mapsto f(\alpha)$ used for the definition of λ.

where: $B_0 = 235.8\ 10^{-3}\ mN/m$; $b = -0.625$; $\nu = 1.256$ and $T_c = 647.096K$ (water critical temperature). $\varphi \in [0,1]$ depends on the nucleation type : homogeneous nucleation occurs when $\varphi = 1$, whereas heterogeneous nucleation occurs when φ is in $]0,1[$. In the simplified model (80), we have (theoreticaly) only two parameters to define: a_0 in (Pa.s), homogeneous to a dynamical viscosity, and $\varphi \in [0,1]$.

We make the assumption that air and vapor act like impurities, enhancing to vaporize liquid water. Therefore, we define φ as:

$$\varphi = \begin{cases} 1 & \text{if } y_v + y_a < 10^{-9}, \\ (y_v + y_a)^2 & \text{otherwise.} \end{cases} \tag{83}$$

a_0 is estimated as:

$$a_0 = \mathcal{P} \times \mathcal{T}, \quad \mathcal{P} \text{ in bar}, \mathcal{T} \text{ in s}, \tag{84}$$

with $\mathcal{P}$ taken equal to 1 bar and $\mathcal{T} = 4.389m/1481\ m.s^{-1}$ s is chosen as an estimation of the time when the depressurization wave will reach the wall of the tube.

Taking $\lambda = t_{nuc}$ seems relevant, while the flow is mainly made of liquid, because the model is related to the very first bubbles appearing at the beginning of the vaporization. Some criterion has to be chosen, to activate or not out-of-equilibrium effects, depend-

ing on the vapor quantity in the flow as well as ΔP (describing how far is the flow from thermodynamical equilibrium after the convection step). Moreover, the time scale is regularized through a cosine function, to avoid too sharp discontinuities. More precisely, λ is chosen as follows:

$$\lambda = \begin{cases} t_{nuc} & \text{if } 0.01bar < \Delta P < 150bar,\ {y_v}^{eq} - y_v < -10^{-6} \text{ and } y_v < 10^{-2}, \\ \tilde{t_{nuc}} & \text{if } 0.01bar < \Delta P < 150bar \text{ and } {y_v}^{eq} - y_v < -10^{-6} \text{ and } 5.0 \times 10^{-3} < y_v < 10^{-2}, \\ 0 & \text{otherwise.} \end{cases} \tag{85}$$

with

$$\tilde{t_{nuc}} = t_{nuc} \cos\left(\frac{(y_v - 5 \times 10^{-3})\pi}{(10^{-2} - 5 \times 10^{-3})2}\right).$$

All the previous threshold values are not based on physical considerations, so that some improvements should be made to propose a more physically relevant model.

5.2.3 Numerical results

Figure 13 shows some results otained with $y_a = 5 \times 10^{-5}$ in the liquid water: three simulations (with $\lambda = 0$, $\lambda = t_{toy}$ and $\lambda = t_{nuc}$) are compared. Out-of-equilibrium simulations enable to get an undershoot for the pressure, below the saturation pressure (around $\simeq 70bar$ for t_{toy} and $\simeq 20bar$ for t_{nuc}), as observed in the experiment around $\simeq 60bar$ (see figure 13a). Moreover, for both out-of-equilibrium simulations, the last depressurisation is correctly delayed, compared with the at-equilibrium simulation, around $\simeq 0.15s$. These results thus highlight the importance of out-of-equilibrium effects to get realistic results.

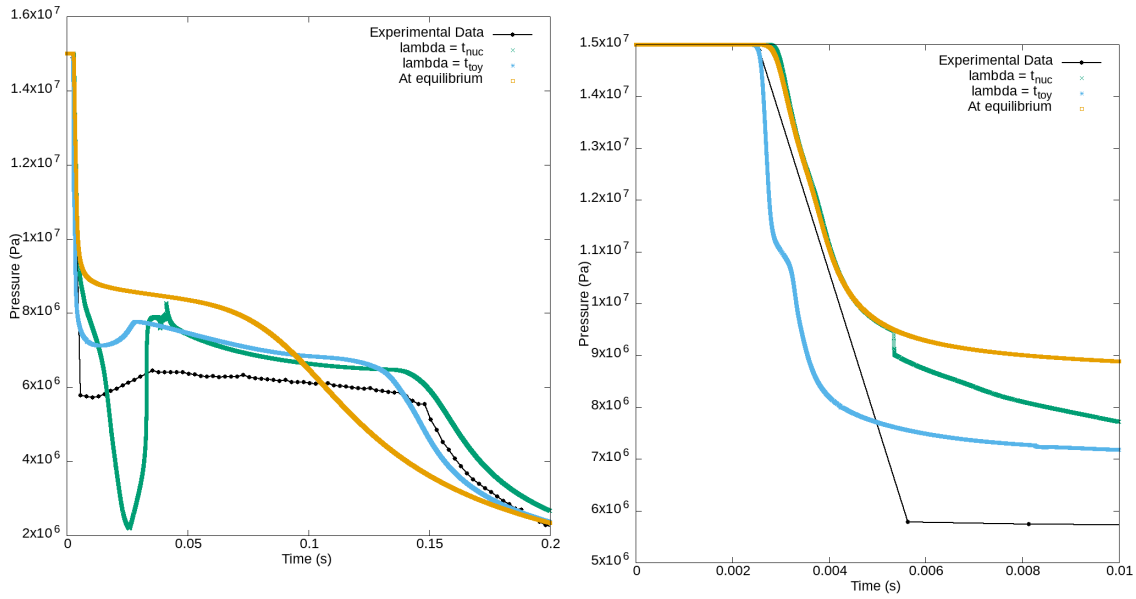

(a) Comparison between simulations and experimental data.

(b) Zoom on the first miliseconds.

Figure 13: Pressure (Pa) within time (s) at point P1 (see figure 9): at-equilibrium simulation ($\lambda = 0$) and out-of-equilibrium simulation ($\lambda = t_{toy}$, see (79) or $\lambda = t_{nuc}$, see (80)), using NASG-CK EOS for the liquid.

Conclusion

The homogeneous model based on (18) and already studied in (25) has been implemented by using a quite realistic phasic equation of state for the liquid water: an extension of the Noble-Able stiffened gas (26), modified with the Chemkin EOS (27), as proposed in (28). As in (23; 47), the convective part of the model is discretized using the scheme proposed in (44) which appeared to be robust and accurate. In fact, for the present model, the main difficulty arises with the computation of the thermodynamical equilibrium: that is why the algorithms have been carefully detailed in this work. Coping with the evanescent phases is more tricky than for liquid-vapor models. This is due to the fact that the number of situations to handle is more important that the threshold fractions may be too close to the thermodynamical equilibrium in some configurations.

The complete scheme has been first verified on Riemann problems, even when considering the source terms for equilibrium configurations as in (23). Then, simulations based on the SUPERCANON experiment (46) have been presented. In pure liquid, with a realistic EOS such as the NASG-CK EOS, the sound speed seems overestimated with respect to the experimental measurements of SUPERCANON. Adding a small amount of air enables to recover a correct speed of propagation of the depressurization wave. More generally, the mass fraction of air y_a is a key parameter, which has a strong influence on the final results. Taking into account out-of-equilibrium effects, through the definition of a time scale λ describing the return towards thermodynamical equilibrium, enables to obtain qualitatively correct results compared with the experiments. The proposition of $\lambda = t_{nuc}$ should still be improved, based on some physical considerations. In particular, t_{nuc} is relevant for small vapor fraction and it should be coupled with an other physical model for high vapor fraction.

Acknowledgements

The last author receives financial support by ANRT through an EDF/CIFRE grant number 2017/0476. Computational facilities were provided by EDF. The authors thank Jean-Marc Hérard for his useful advice.

Appendices

6 Concavity of the intensive entropies

Here, we recall the consequences of property 1 in terms of concavity, without detailing the proofs. We refer to (24) for detailed proofs, adapted from (32; 35; 30), in a very similar case: indeed, in (24), the model deals with a three-phase flow model describing three immiscible components, which leads to the same definition as (18) for the mixture entropy.

Property 11 (Concavity of S)

$W \in \Omega \mapsto S(W)$ is concave. Moreover, if we consider the manifold $\tilde{\Omega} = \{W \in \Omega / \mathcal{M} > 0 \text{ is fixed}\}$, then $W \in \tilde{\Omega} \mapsto S(W)$ is strictly concave.

Property 12 (Concavity of s_k)

$(\tau_k, e_k) \in (\mathbb{R}^{+,*}, \mathbb{R}^*) \mapsto s_k(\tau_k, e_k)$ is concave.

Property 13 (Concavity of s)

We recall the notation $Y = (\alpha_v, y_v, y_a, z_v, z_a)$.

(I) : For a given (τ, e), $Y \in [0,1]^5 \mapsto s(Y, \tau, e)$ is strictly concave. This property implies that s admits a unique maximum reached on a fraction set $\bar{Y}$, which is defined as the thermodynamical equilibrium.

(II) : For a given $Y \in [0,1]^5$, $(\tau, e) \mapsto s(Y, \tau, e)$ is strictly concave. This property allows to define the shock wave in a unique manner.

7 Coefficients for NASG-CK EOS and SG EOS

Coefficients	Liquid NASG-CK
A_l (dimensionless)	4.69738865636393e+01
B_l (K^{-1})	-4.19269571479452e-01
C_l (K^{-2})	1.70702143968620e-03
D_l (K^{-3})	-3.04805662517983e-06
E_l (K^{-4})	2.02814588067819e-09
F_l (K)	-2.523528536614e+06/R
G_l (dimensionless)	-7.431869850561e+04/R
γ_l (dimensionless)	1.22208363133609e+00
$C_{v,l}$ $(JK^{-1}kg^{-1})$	3.51131133724707e+03
Π_l (Pa)	7.01704922088062e+08
b_l (m^3kg^{-1})	6.20558682225980e-04

Table 7.1: Coefficients for Noble-Able Chemkin EOS (50), for liquid water.

Coefficients	Liquid SG
γ (dimensionless)	1.39864082368510
C_v $(JK^{-1}kg^{-1})$	3.19641035947920e+03
Q (Jkg^{-1})	-1.357495682920e+06
Π (Pa)	4.79690712132593e+08
k $(JK^{-1}kg^{-1})$	5.962461101053e+01

Table 7.2: Coefficients for stiffened gas EOS, for liquid water, obtained from the optimization process in chapter 2 of (37), where $k = C_v \ln(C_v) + C_v(\gamma - 1)\ln(C_v(\gamma - 1)) + s_0$.

Coefficients	Vapor SG
γ (dimensionless)	1.15442237458290
$C_v\ (JK^{-1}kg^{-1})$	2.91668522329726e+03
$Q\ (Jkg^{-1})$	1.25942536895827e+06
$\Pi\ (Pa)$	-3.24993579473092e+02
$k\ (JK^{-1}kg^{-1})$	-7.77026092439033e+03

Table 7.3: Coefficients for stiffened gas EOS, for vapor, obtained from the optimization process in chapter 2 of (37), where $k = C_v \ln(C_v) + C_v(\gamma - 1)\ln(C_v(\gamma - 1)) + s_0$.

Coefficients	Air SG
γ (dimensionless)	1.4
$C_v\ (JK^{-1}kg^{-1})$	719.0
$Q\ (Jkg^{-1})$	0
$\Pi\ (Pa)$	0
$k\ (JK^{-1}kg^{-1})$	0

Table 7.4: Coefficients for stiffened gas EOS, for air, considered as a perfect gas

8 Initial data for Riemann problems test cases

Data	Left state	Intermediate state	Right state
α	9.83232179608806 10^{-1}	9.87041861906529 10^{-1}	9.87041861906529 10^{-1}
y	3.17380286565343 10^{-2}	4.03113857253491 10^{-2}	4.03113857253491 10^{-2}
z	4.91959192421520 10^{-1}	5.44567894139035 10^{-1}	5.44567894139035 10^{-1}
y_a	5.0 10^{-2}	6.18446225562366 10^{-2}	6.18446225562366 10^{-2}
z_a	8.83504641470457 10^{-2}	9.77984087865951 10^{-2}	9.77984087865951 10^{-2}
τ (m^3/kg)	5.4427805669757310^{-2}	6.886350393192439 10^{-2}	6.89635039319242 10^{-2}
u (m/s)	1.0	1.0	-2.15013291878029
P (Pa)	1.86680031787657 10^5	1.86680031787657 10^5	8.74466577184921 10^4

Table 8.1: Out-of-equilibrium test case 1. $\sigma = 2170.29190638504$ m/s

Data	Left state	Intermediate state	Right state
α	2.83455356934630 10^{-1}	6.11774284813328 10^{-1}	3.99122663398670 10^{-1}
y	4.25625125846829 10^{-3}	8.70625146760066 10^{-3}	1.0 10^{-2}
z	1.51011070725486 10^{-2}	2.91840921657732 10^{-2}	3.35291837019411 10^{-2}
y_a	2.0 10^{-2}	3.0 10^{-2}	3.0 10^{-2}
z_a	9.24831478659724 10^{-3}	1.32498062560992 10^{-2}	1.32417151719985 10^{-2}
τ (m^3/kg)	1.6382140748807462 10^{-3}	1.9485538689275692 10^{-3}	2.080256962546277 10^{-3}
u (m/s)	1.0	1.0	-9.71690290715716
P (Pa)	8.00000000000805 10^6	7.99999999999713 10^6	7.12794753132892 10^6

Table 8.2: At-equilibrium test case 2 (smooth case) : $\sigma = 159.557115470034$ m/s

Data	Left state	Intermediate state	Right state
α	4.55806467748821 10^{-1}	6.35814523035530 10^{-1}	9.88240646295054 10^{-1}
y	2.79348914129385 10^{-2}	5.74662402110775 10^{-2}	1.0 10^{-1}
z	7.30830106253936 10^{-2}	1.44714572786685 10^{-1}	4.11152591599341 10^{-1}
y_a	5.0 10^{-2}	9.0 10^{-2}	9.0 10^{-2}
z_a	1.81366554653765 10^{-2}	3.15417178714970 10^{-2}	4.39343919538099 10^{-2}
τ (m^3/kg)	2.18882462814298 10^{-3}	3.0386914611470485 10^{-3}	7.55537631384807 10^{-2}
u (m/s)	1.0	1.0	-1028.59799314035
P (Pa)	1.49999999999975 10^7	1.50000000000035 10^7	3.21668487111682 10^5

Table 8.3: At-equilibrium test case 3 (high pressure gap) : $\sigma = 44.1445568183537$ m/s

9 Algorithms to compute the thermodynamical equilibrium

Here, we present the four auxiliary algorithms, called in the main algorithm 1. They are built among the same principles in (14), enabling to compute the thermodynamical equilibrium, depending on the fields which are actually present in the mixture, as explained in properties 3 and 4. Note that ALGORITHM 2 is independent from the choice of phasic EOS, whereas the other algorithms **take advantage of the particular form of the stiffened gas EOS used for the vapor and the non-condensable gas** (see remark 6).

ALGORITHM 2 (Equilibrium l and v) — Arguments: (τ, e).
Liquid-vapor equilibrium satisfies:

$$\begin{aligned} P_l(\tau_l, e_l) &= P_v(\tau_v, e_v) = \bar{P}; \\ T_l(\tau_l, e_l) &= T_v(\tau_v, e_v) = \bar{T}; \\ \mu_l(P_l, T_l) &= \mu_v(P_v, T_v), \end{aligned} \tag{86}$$

with $\tau_k = \frac{\alpha_k}{y_k}\tau$ and $e_k = \frac{z_k}{y_k}e$ for $k = l, v$.

Instead of looking for fractions $\bar{\alpha}_v$, $\bar{y}_v$ and $\bar{z}_v$ satisfying (86), the unknowns $\bar{P}$, $\bar{T}$ and $\bar{y}_v$

are considered. Last equation from (86):

$$\mu_l(\bar{P}, \bar{T}) = \mu_v(\bar{P}, \bar{T}), \tag{87}$$

enables to implicitely define the function for the saturation temperature $\bar{P} \to \bar{T} = T_{sat}(\bar{P})$. In practice, for each tested $\bar{P}$, the saturation temperature $\bar{T}$ is then obtained by using a secant method to solve (87).

Our entry arguments (τ, e) give us two more equations due to the miscibility constraints (8) and (9), both depending on $\bar{y}_v$, which are:

$$\begin{aligned} \tau &= (1 - \bar{y}_v) \times \tau_l(\bar{P}, T_{sat}(\bar{P})) \\ &+ \bar{y}_v \times \tau_v(\bar{P}, T_{sat}(\bar{P})), \\ e &= (1 - \bar{y}_v) \times e_l(\bar{P}, T_{sat}(\bar{P})) \\ &+ \bar{y}_v \times e_v(\bar{P}, T_{sat}(\bar{P})). \end{aligned} \tag{88}$$

First equation of (88) leads to an explicit formula for $\bar{y_v}$, as a function of $\bar{P}$:

$$\begin{aligned} \bar{y_v} &= \bar{y}_v(\bar{P}) \\ &= \frac{\tau - \tau_l(\bar{P}, T_{sat}(\bar{P}))}{\tau_v(\bar{P}, T_{sat}(\bar{P})) - \tau_l(\bar{P}, T_{sat}(\bar{P}))}. \end{aligned} \tag{89}$$

The resolution is finally achieved with a secant method by looking for $\bar{P}$ verifying:

$$\begin{aligned} e &= (1 - \bar{y}_v(\bar{P})) \times e_l(\bar{P}, T_{sat}(\bar{P})) \\ &+ \bar{y}_v(\bar{P}) \times e_v(\bar{P}, T_{sat}(\bar{P})), \end{aligned} \tag{90}$$

using the previous definition (89) for $\bar{y}_v(\bar{P})$.

ALGORITHM 3 (Equilibrium *l*, *v* and *a*) — Arguments: (y_a, τ, e).
Thermodynamical equilibrium (27) is characterized in (τ, e)-plane, as depicted in property 3, by:

$$\begin{aligned} &P_l(\tau_l, e_l) = P_v(\tau_v, e_v) + P_a(\tau_a, e_a) = \bar{P}; \\ &T_l(\tau_l, e_l) = T_v(\tau_v, e_v) = \bar{T}; \\ &T_v(\tau_v, e_v) = T_a(\tau_a, e_a) = \bar{T}; \\ &\mu_l(P_l(\tau_l, e_l), T_l(\tau_l, e_l)) = \mu_v(P_v(\tau_v, e_v), T_v(\tau_v, e_v)); \end{aligned} \tag{91}$$

As already explained in section 3.3, instead of looking for $\bar{\alpha}_v$, $\bar{y}_v$, $\bar{z}_v$ and $\bar{z}_a$ satisfying (91), the following unknows are considered in pressure-temperature plane: $\bar{P}_v$, $\bar{P}_a$, $\bar{T}$ and $\bar{y}_v$. Miscibility constraints (7) enable to get a system equivalent to system (91) in pressure-temperature plane:

$$\begin{aligned} \bar{y}_v \times \tau_v(\bar{P}_v, \bar{T}) &= y_a \times \tau_a(\bar{P}_a, \bar{T}); \\ \tau &= (1-\bar{y}_v) \times \tau_l(\bar{P}_v + \bar{P}_a, \bar{T}) \\ &\quad + \bar{y}_v \times \tau_v(\bar{P}_v, \bar{T}); \\ e &= (1-\bar{y}_v) \times e_l(\bar{P}_v + \bar{P}_a, \bar{T}) \\ &\quad + \bar{y}_v \times e_v(\bar{P}_v, \bar{T}) + y_a \times e_a(\bar{P}_a, \bar{T}); \\ &\mu_l(\bar{P}_v + \bar{P}_a, \bar{T}) = \mu_v(\bar{P}_v, \bar{T}). \end{aligned} \tag{92}$$

The previous system is solved as follows, in three steps:

1. Thanks to the particular form of the stiffened gas EOS, the first equation of (92) gives an explicit definition of $\bar{y}_v$ as a function of $\bar{P}_v$ and $\bar{P}_a$:

$$\begin{aligned} \bar{y}_v &= y_a = \frac{C_{v,a}(\gamma_a - 1)}{C_{v,v}(\gamma_v - 1)} \frac{(\bar{P}_v + \Pi_v)}{(\bar{P}_a + \Pi_a)} \\ &= \bar{y}_v(\bar{P}_v, \bar{P}_a). \end{aligned} \tag{93}$$

2. **The stiffened gas formula is used** to compute $\bar{T}$. Indeed, its particular form enables to uncouple $\bar{T}$ and $\bar{y}_v$ in the second equation of (92) :

$$\begin{aligned} \bar{T} &= (\tau - (1 - y_a - \bar{y}_v) b_l) \times \\ &\quad ((1 - y_a - \bar{y}_v) C_{v,l}(\gamma_l - 1) \\ &\quad + y_a C_{v,a}(\gamma_a - 1))^{-1} \\ &= \bar{T}(\bar{P}_v, \bar{P}_a). \end{aligned} \tag{94}$$

3. We still need to solve the following system relatively to $(\bar{P}_v, \bar{P}_a)$, for instance with a

Broyden algorithm:

$$\begin{cases} (f_1): & \mu_l(\bar{P}_v + \bar{P}_a, \bar{T}) = \mu_v(\bar{P}_v, \bar{T}) \\ (f_2): & e = (1 - \bar{y}_v - y_a) \times e_l(\bar{P}_v + \bar{P}_a, \bar{T}) \\ & +\bar{y}_v \times e_v(\bar{P}_v, \bar{T}) + y_a \times e_a(\bar{P}_a, \bar{T}) \\ \text{with:} & \bar{y}_v = \bar{y}_v(\bar{P}_v, \bar{P}_a) \text{ from (93)} \\ \text{and} & \bar{T} = \bar{T}(\bar{P}_v, \bar{P}_a) \text{ from (94)}. \end{cases}$$

A difficulty arising with Broyden algorithm is to propose a relevant starting point. Several choices are tested in the code:

- correlations based on polynomials, obtained with R from large data sets;
- pressures obtained after solving a dichotomy on either (f_1) or (f_2), by fixing either P_v or P_a;
- pressure P_v obtained with the same τ and e but $y_a = 0$.

However, Broyden algorithm may still fail. A double dichotomy on P_v, and then P_a has also been implemented, but it has also a lack of robustness since we may have difficulties to define some explicit bounds for P_v and P_a.

ALGORITHM 4 (Equilibrium *l* and *a*) — Arguments: (τ, e).
In this case:

$$y_v = 0 \qquad ; \qquad y_l = 1 - y_a.$$

Conditions from property 4 are recalled, with $\tau_k = \frac{\alpha_k}{y_k}\tau$ and $e_k = \frac{z_k}{y_k}e$ for $k = l, a$:

$$\begin{aligned} P_l(\tau_l, e_l) &= P_a(\tau_a, e_a) = \bar{P}; \\ T_l(\tau_v, e_v) &= T_a(\tau_a, e_a) = \bar{T}; \end{aligned} \tag{95}$$

Due to our entry arguments (τ, e), unknowns $\bar{P}$, $\bar{T}$ are once more relevant, and miscibility constraints (8) and (9) lead to:

$$\begin{aligned} \tau &= (1 - y_a) \times \tau_l(\bar{P}, \bar{T}) + y_a \times \tau_a(\bar{P}, \bar{T}), \\ e &= (1 - y_a) \times e_l(\bar{P}, \bar{T}) + y_a \times e_a(\bar{P}, \bar{T}). \end{aligned} \tag{96}$$

Due to the particular form of the stiffened gas EOS, the first equation of (96) leads to an explicit definition of $\bar{T}$ as a function of $\bar{P}$:

$$\begin{aligned}\bar{T} &= (\tau - (1-y_a)b_l)\times \\ &\left(\frac{y_a C_{v,a}(\gamma_a - 1)}{\bar{P} + \Pi_a} + \right. \\ &\left. \frac{(1-y_a)C_{v,l}(\gamma_l - 1)}{\bar{P} + \Pi_l}\right)^{-1} \\ &= \bar{T}(\bar{P}),\end{aligned} \tag{97}$$

so that there is only one implicit equation in $\bar{P}$ left:

$$\begin{aligned}&(f): \quad e = (1-y_a)\times e_l(\bar{P}, \bar{T}(\bar{P})) + y_a \times e_a(\bar{P}, \bar{T}(\bar{P})), \\ &\text{with:} \quad \bar{T} = \bar{T}(\bar{P}) \text{ from (97)}.\end{aligned} \tag{98}$$

The resolution is finally achieved by looking for $\bar{P}$ verifying equation (98) with a secant method.

ALGORITHM 5 (Equilibrium v and a) — Arguments: (τ, e).

In this case:

$$y_l = 0 \qquad ; \qquad y_v = 1 - y_a.$$

Only one condition is obtained from property 4:

$$\bar{T} = T_v(\tau_v, e_v) = T_a(\tau_a, e_a). \tag{99}$$

In pressure-temperature plane, the miscibility constraints from hypothesis 6 lead to the following condition:

$$\tau = y_a \tau_a(\bar{P}_a, \bar{T}) = (1-y_a)\tau_v(\bar{P}_v, \bar{T}),$$

which implies (**since we use stiffened gas EOS**):

$$\bar{T} = \frac{(e - (y_a Q_a + (1-y_a)Q_v)}{y_a C_{v,a} + (1-y_a)C_{v,v}} + (\Pi_a + \Pi_v)\tau.$$

Finally, $\bar{P}_a$ and $\bar{P}_v$ can be explicitly deduced thanks to **the stiffened gas phasic EOS**:

$$\bar{P}_k = \frac{y_k C_{v,k}(\gamma_k - 1)\bar{T}}{\tau} - \Pi_k, \quad k = v, a.$$

10 Analytical solutions for the model

For the sake of readibility, let us highlight that all the variables are initialized since y_a and phasic pressures and temperatures are given through the following function INIT$(y_a, P_l, P_v, P_a, T_l, T_v$

ALGORITHM 6 (Initialization) — INIT$(y_a, P_l, P_v, P_a, T_l, T_v, T_a)$ enables to compute: $(\alpha, y_v, z_v, z_a, \tau, e, P, T$ from $(y_a, P_l, P_v, P_a, T_l, T_v, T_a)$:

1. Using the phasic EOS:
   - $\tau_l = b_l + \dfrac{C_{v,l}(\gamma_l - 1)T_l}{P_l + \Pi_l}$ and $\tau_k = \dfrac{C_{v,k}(\gamma_k - 1)T_k}{P_k + \Pi_k}$ for $k = v, a$.
   - $e_l = RT_l(A_l + \frac{B_l}{2}T_l + \frac{C_l}{3}T_l^2 + \frac{D_l}{4}T_l^3 + \frac{E_l}{5}T_l^4 + \frac{F_l}{T_l}) - P_l(\tau_l - b_l)$ and $e_k = C_{v,k}T_k + Q_k + (\tau_k - b_k)\Pi_k$ for $k = v, a$.
2. Using miscibility constraints (7):
   - $y_v = y_a\dfrac{\tau_a}{\tau_v}$ so that $y_l = 1 - y_a - y_v$;
   - $\tau = y_l\tau_l + y_a\tau_a$;
   - $e = y_l e_l + y_v e_v + y_a e_a$.
3. Using the definition of phasic fractions:
   - $\alpha = \alpha_v = \alpha_a = y_v\dfrac{\tau_v}{\tau}$;
   - $z_k = y_k\dfrac{e_k}{e}$ for $k = v, a$.
4. Using the definition of mixture pressure and temperature (38) and (39):

$$P = \frac{(1-\alpha_v)\frac{P_l}{T_l} + \alpha_v(\frac{P_v}{T_v} + \frac{P_a}{T_a})}{\frac{1-z_v-z_a}{T_l} + \frac{z_v}{T_v} + \frac{z_a}{T_a}};$$

$$\frac{1}{T} = \frac{1-z_v-z_a}{T_l} + \frac{z_v}{T_v} + \frac{z_a}{T_a}.$$

Our methods to build analytical Riemann problems are now presented in the two following algorithms.

ALGORITHM 7 (Out-of-equilibrium Riemann problem) — Approach:

1. We define the left state W^L:
   - by choosing U^L, P_k^L and T_k^L for $k \in \mathcal{K}$;
   - by deducing the other quantities $\alpha_v^L, y_v^L, z_v^L, z_a^L, e^L, \tau^L, P^L$ and T^L from $\text{INIT}(y_a^L, P_l^L, P_v^L, P_a^L, T_l^L, T$
2. Then, we define the intermediate state W^*:
   - by imposing $U^* = U^L$ (due to (43) through a contact);
   - by choosing P_k^* and T_k^* for $k \in \mathcal{K}$;
   - by finding thanks to dichotomy algorithm y_a^* so that

     $$P^*(y_a^*) = P^L \text{ (due to (43) through a contact).}$$

     Indeed, for each tested $\tilde{y}_a^*$, we use $\text{INIT}(\tilde{y}_a^*, P_l^*, P_v^*, P_a^*, T_l^*, T_v^*, T_a^*)$, so that we get a value for $\tilde{P}^* = \tilde{P}^*(\tilde{y}_a^*)$.
   - once y_a^* is found, the other quantities are computed with $\text{INIT}(y_a^*, P_l^*, P_v^*, P_a^*, T_l^*, T_v^*, T_a^*)$.
3. Last, we define the right state W^R:
   - by imposing $\alpha_v^R = \alpha_v^*$, $y_v^R = y_v^*$, $y_a^R = y_a^*$, $z_v^R = z_v^*$ and $z_a^R = z_a^*$ (due to (43) through a shock);
   - by arbitrarely imposing τ^R;
   - by looking for e^R verifying the last Rankine-Hugoniot equation through a shock:

     $$e^R - e^* + (\tau^R - \tau^*)\frac{P^R(e^R, ...) + P^*}{2} = 0$$

     where, using (38),

     $$P^R = P^R(e^R, \tau^R, \alpha_v^R, y_v^R, y_a^R, z_v^R, z_a^R);$$

   - and last by deducing with (43) $J^2 = \dfrac{-P^R + P^*}{\tau^R - \tau*}$, and then $U^R = U^* - \dfrac{P^R - P*}{J}$ and $\sigma = U^R - J\tau^R$.

ALGORITHM 8 (At-equilibrium Riemann problem) — Approach:

1. We define the left state W^L:
   - by choosing U^L;
   - by choosing P_k^L and T_k^L to comply with thermodynamical equilbrium, so that:
   $$P_l^L = P_v^L + P_a^L \quad \text{and} \quad T_k^L = T_{sat}(P_v^L, P_a^L)\ \forall k \in \mathcal{K};$$
   - by deducing the other quantities $\alpha_v^L, y_v^L, z_v^L, z_a^L, e^L, \tau^L, P^L$ and T^L from $\text{INIT}(y_a^L, P_l^L, P_v^L, P_a^L, T_l^L, T$
2. Then, we define the intermediate state W^*:
   - by imposing $U^* = U^L$ (due to (43) through a contact);
   - by choosing P_k^* and T_k^* to comply with thermodynamical equilibrium) i.e. by choosing
   $$P_l^* = P_l^L \quad \text{and} \quad P_k^* \neq P_k^L,$$
   so that:
   $$P_v^L + P_a^L = P_v^* + P_a^* \text{ and}$$
   $$T_k^L = T_{sat}(P_v^*, P_a^*) \quad \forall k \in \mathcal{K};$$
   - and then, by deducing the other quantities $\alpha_v^*, y_v^*, z_v^*, z_a^*, e^*, \tau^*, P^*$ and T^* from $\text{INIT}(y_a^*, P_l^*, P_v^*, P_a^*, T_l^*, T_v^*, T_a^*)$.
3. Last, we define the right state W^R:
   - by imposing $y_a^R = y_a^*$ (due to (43) through a shock);
   - by arbitrarely defining $y_v^R \neq y_v^*$;
   - by looking for P_v^R verifying the last Rankine-Hugoniot equation through a shock:
   $$e^R(P_v^R, ...) - e^* + (\tau^R(P_v^R, ...) - \tau^*) \times \frac{P_v^R + P_a^R(P_v^R, ...) + P^*}{2} = 0;$$
   We detail the terms from the previous equation:

– as y_v^R and y_a^R are given, P_a^R is imposed by P_v^R through the constraints $y_a\tau_a = y_v\tau_v$ for SG EOS, so that:

$$\begin{aligned} P_a^R &= \frac{y_a^R}{y_v^R}\frac{C_{v,a}(\gamma_a - 1)}{C_{v,v}(\gamma_v - 1)}(P_v^R + \Pi_v) - \Pi_a \\ &= P_a^R(P_v^R); \end{aligned}$$

– once P_v^R and P_a^R are known, T^R is defined as

$$T^R = T_{sat}(P_v^R, P_a^R),$$

by equalizing the chemical potentials via a dichotomy algorithm:

$$\mu_l(P_v^R + P_a^R(P_v^R), T^R) = \mu_v(P_v^R, T^R).$$

– e^R and τ^R can be evaluated with P_v^R, P_a^R and T^R thanks to phasic EOS (cf ALGORITHM 6):

$$e^R = \sum_{k\in\mathcal{K}} y_k^R e_k(P_k^R, T^R(P_v^R));$$

$$\begin{aligned} \tau_R &= (1 - y_a^R - y_v^R)\tau_l(P_v^R + P_a^R(P_v^R), T^R(P_v^R)) \\ &\quad + y_v^R\tau_v(P_v^R, T^R(P_v^R)). \end{aligned}$$

- Last by deducing with (43) $J^2 = \dfrac{-P^R + P^*}{\tau^R - \tau*}$, and then $U^R = U^* - \dfrac{P^R - P*}{J}$ and $\sigma = U^R - J\tau^R$.

Remark 8 — We draw the reader's attention on the jump for the fractions within the shock for an at-equilibrium Riemann problem: the evolution of Y is far more complex as a simple convection equation as it is the case for an out-of-equilibrium Riemann problem. Therefore, the fractions are no more constant in a shock when we consider an at-equilibrium Riemann problem.

11 Empirical method to estimate NASG-CK coefficients

In order to estimate the coefficients for a NASG-CK EOS, an empirical method is proposed, in the same spirit as what was proposed in (41) for the stiffened gas EOS:

1. A point (P_0, T_0) of the physical domain is chosen as reference point. It should be representative of the aimed simulation. The following thermodynamical quantities are obtained with the IAPWS-97 formulation: the specific volume $\tau_0(P_0, T_0)$, the thermal expansion coefficient $\alpha_{P,0}(P_0, T_0)$, the specific heat capacity at constant volume $C_{v,0}(P_0, T_0)$ as well as the sound speed $c_0(P_0, T_0)$.

2. ${C_p}^{NASG-CK}$ is computed with formula (51) as ${C_p}^{NASG-CK} = {C_p}^{NASG-CK}(T_0)$, using coefficients A_l, B_l, C_l, D_l and E_l obtained by a minimization of the L1-error with respect to IAPWS on a large liquid domain.

3. Recalling formula for NASG-CK EOS:

$$c^2 = \frac{1}{T\alpha_P^2}\left(\frac{1}{(\gamma-1)C_v} - \frac{1}{C_p(T)}\right)^{-1},$$

   $\mathcal{A}_l = (\gamma^{NASG-CK} - 1) \times {C_v}^{NASG-CK}$ is deduced from c_0 and $\alpha_{P,0}$:

$$\begin{aligned}\mathcal{A}_l &= (\gamma^{NASG-CK} - 1) \times {C_v}^{NASG-CK} \\ &= \left(\frac{1}{c_0^2 {\alpha_{P,0}}^2 T_0} + \frac{1}{{C_p}^{NASG-CK}}\right)^{-1}.\end{aligned}$$

4. ${C_v}^{NASG-CK}$ is taken equal as the IAPWS value at P_0 and T_0:

$${C_v}^{NASG-CK} = C_{v,0}(P_0, T_0),$$

   so that $\gamma^{NASG-CK}$ is obtained through the relation

$$\gamma^{NASG-CK} = \frac{\mathcal{A}_l}{C_{v,0}(P_0, T_0)} + 1.$$

5. Then, using α_P definition (51), we get:

$$\mathcal{B}_l = b_l \times (P_0 + \Pi_l) =$$
$$(\frac{1}{\alpha_{P,0}} - T_0) \times (\gamma^{NASG-CK} - 1) \times {C_v}^{NASG-CK}.$$

6. Π_l and b_l are deduced from τ_0 and $\mathcal{B}_l$:

$$\Pi_l = \frac{\mathcal{B}_l + T_0 \times \mathcal{A}_l}{\tau_0} - P_0$$

and

$$b_l = \frac{\mathcal{B}_l}{(P_0 + \Pi_l)}.$$

7. Last, F_l and G_l are obtained as follows:

   - $\tilde{\mu_l}$ is computed using a lot of points $(P_l, T_l = T^{sat}_{IAPWS}(P_l))$, by taking $F_l = G_l = 0$;
   - thanks to a linear regression on $\tilde{\mu_l} - \mu_v$, we get: $\tilde{\mu_l} - \mu_v \simeq c_1 + T_l c_2$, which can be seen as a linear correction for $\tilde{\mu_l}$;
   - we then choose:

$$F_l = -\frac{c_1}{R} \quad ; G_l = \frac{c_2}{R}.$$

In practice, the previous method is used in this work for a liquid reference point $(P_0 = 80bar, T_0 = 425K)$.

Note that this method works quite well far from the saturation curve (that is to say, according to our tests, for a given pressure P_0, a temperature $T_0 < T^{sat}(P_0) - 40K$ shoud be chosen): otherwise, it may lead to a $b_l < 0$, which is not physically relevant.

References

[1] IRSN, Accidents graves pouvant affecter un réacteur à eau pressurisée. (2011).
URL https://www.irsn.fr/fr/connaissances/installations_nucleaires/les-accidents-nucleaires/

[2] J. Huang, J. Zhang, L. Wang, Review of vapor condensation heat and mass transfer in the presence of non-condensable gas, Applied thermal engineering 89 (2015) 469–484. doi:https://doi.org/10.1016/j.applthermaleng.2015.06.040.

[3] M. Bachmann, S. Müller, P. Helluy, H. Mathis, A Simple Model for Cavitation with Non-condensable Gases, in: Hyperbolic Problems: Theory, Numerics and Applications, Vol. 18, World Scientific, 2012, pp. 289 – 296. doi:10.1142/9789814417099_0024.
URL https://hal.archives-ouvertes.fr/hal-01420483

[4] R. Meignen, B. Raverdy, S. Picchi, J. Lamome, The challenge of modeling fuel–coolant interaction: Part ii–steam explosion, Nuclear Engineering and Design 280 (2014) 528–541. doi:http://dx.doi.org/10.1016/j.nucengdes.2014.08.028.

[5] F. Barre, M. Bernard, The CATHARE code strategy and assessment, Nuclear engineering and design 124 (3) (1990) 257–284. doi:https://doi.org/10.1016/0029-5493(90)90296-A.

[6] M. Baer, J. Nunziato, A two-phase mixture theory for the deflagration-to-detonation transition (DDT) in reactive granular materials, Journal of Multiphase Flows 12 (1986) 861–889. doi:https://doi.org/10.1016/0301-9322(86)90033-9.

[7] J. Glimm, D. Saltz, D. Sharp, Two-pressure two-phase flow, in: Advances In Nonlinear Partial Differential Equations And Related Areas: A Volume in Honor of Professor Xiaqi Ding, World Scientific, 1998, pp. 124–148. doi:https://doi.org/10.1142/9789812815811_0008.

[8] H. Jin, J. Glimm, D. Sharp, Compressible two-pressure two-phase flow models, Physics letters A 353 (6) (2006) 469–474. doi:https://doi.org/10.1016/j.physleta.2005.11.087.

[9] F. Coquel, T. Gallouët, J.-M. Hérard, N. Seguin, Closure laws for a two-fluid two-

pressure model, Comptes Rendus Mathématique 334 (10) (2002) 927–932.
URL https://hal.archives-ouvertes.fr/hal-01484345

[10] S. Gavrilyuk, R. Saurel, Mathematical and numerical modeling of two-phase compressible flows with micro-inertia, J. Comput. Phys. 175 (1) (2002) 326–360. doi:http://dx.doi.org/10.1006/jcph.2001.6951.

[11] A. K. Kapila, R. Menikoff, J. B. Bdzil, S. F. Son, D. S. Stewart, Two-phase modeling of deflagration-to-detonation transition in granular materials: Reduced equations, Physics of Fluids 13 (10) (2001) 3002–3024. doi:https://doi.org/10.1063/1.1398042.

[12] G. Allaire, S. Clerc, S. Kokh, A five-equation model for the numerical simulation of interfaces in two-phase flows, Comptes Rendus de l'Académie des Sciences - Series I - Mathematics 331 (12) (2000) 1017 – 1022.
URL http://www.sciencedirect.com/science/article/pii/S0764444200017535

[13] G. Faccanoni, Study of a Fine Model of Liquid-Vapor Phase Change. Contribution to the Boiling Crisis Study., Ph.D. thesis, Ecole Polytechnique X (Nov. 2008).
URL https://pastel.archives-ouvertes.fr/tel-00363460

[14] G. Faccanoni, S. Kokh, G. Allaire, Modelling and Simulation of Liquid-Vapor Phase Transition in Compressible Flows Based on Thermodynamical Equilibrium., Mathematical Modelling and Numerical Analysis 46 (05) (2012) 1029–1054.
URL https://hal.archives-ouvertes.fr/hal-00976983

[15] H. Guillard, A. Murrone, A five equation reduced Model for compressible two phase flow problems, Tech. Rep. RR-4778, INRIA (Mar. 2003).
URL https://hal.inria.fr/inria-00071808

[16] P. Downar-Zapolski, Z. Bilicki, L. Bolle, J. Franco, The non-equilibrium relaxation model for one-dimensional flashing liquid flow, International Journal of Multiphase Flow 22 (3) (1996) 473–483. doi:https://doi.org/10.1016/0301-9322(95)00078-X.

[17] E. Faucher, J.-M. Hérard, M. Barret, C. Toulemonde, Computation of flashing flows in variable cross-section ducts, International Journal of Computational Fluid Dynamics 13 (3) (2000) 365–391.
URL https://hal.archives-ouvertes.fr/hal-01580046

[18] T. Barberon, P. Helluy, Finite volume simulation of cavitating flows, Computers and Fluids 34 (7) (2005) 832–858.
URL https://hal.archives-ouvertes.fr/hal-00139597

[19] G. Berthoud, Vapor explosions, Annual Review of Fluid Mechanics 32 (1) (2000) 573–611. doi:https://doi.org/10.1146/annurev.fluid.32.1.573.

[20] J.-M. Hérard, H. Mathis, A three-phase flow model with two miscible phases, ESAIM: Mathematical Modelling and Numerical Analysis 53, 1373-1389 (Apr. 2019).
URL https://hal.archives-ouvertes.fr/hal-01976938

[21] J.-M. Hérard, O. Hurisse, L. Quibel, Simulations of liquid-vapor water flows with incondensable gases on the basis of a two-fluid model (2020).

[22] O. Hurisse, Numerical simulations of steady and unsteady two-phase flows using a homogeneous model, Computers and Fluids 152 (2017) 88–103.
URL https://hal.archives-ouvertes.fr/hal-01489039

[23] P. Helluy, O. Hurisse, L. Quibel, Assessment of numerical schemes for complex two-phase flows with real equations of state, Computers and Fluids 196 (104347) (Jan. 2020).
URL https://hal.archives-ouvertes.fr/hal-02315038

[24] O. Hurisse, L. Quibel, A homogeneous model for compressible three-phase flows involving heat and mass transfer., ESAIM: Proceedings and Surveys 66 (2019) 84–108.
URL https://hal.archives-ouvertes.fr/hal-01976903

[25] H. Mathis, A thermodynamically consistent model of a liquid-vapor fluid with a gas, ESAIM: Mathematical Modelling and Numerical Analysis 53 (1) (2019) 63–84. doi:https://doi.org/10.1051/m2an/2018044.

[26] O. Le Métayer, R. Saurel, The Noble-Abel Stiffened-Gas equation of state, Physics of Fluids 28 (2016) 046102. doi:10.1063/1.4945981.
URL https://hal.archives-ouvertes.fr/hal-01305974

[27] R. J. Kee, F. M. Rupley, E. Meeks, J. A. Miller, CHEMKIN-III: A FORTRAN chemical kinetics package for the analysis of gas-phase chemical and plasma kinetics, Tech. rep., Sandia National Labs., Livermore, CA (United States) (1996).
URL https://www.osti.gov/biblio/481621

[28] P. Boivin, M. Cannac, O. Le Metayer, A thermodynamic closure for the simulation of multiphase reactive flows, International Journal of Thermal Sciences 137 (2019) 640–649.
URL https://hal.archives-ouvertes.fr/hal-01981954

[29] P. Helluy, O. Hurisse, L. Quibel, Simulation of a liquid-vapour compressible flow by a Lattice Boltzmann Method, working paper or preprint (Jan. 2020).
URL https://hal.archives-ouvertes.fr/hal-02451368

[30] J. Jung, Numerical simulations of two-fluid flow on multicores accelerator, Ph.D. thesis, Université de Strasbourg (Oct. 2013).
URL https://tel.archives-ouvertes.fr/tel-00876159

[31] P. Helluy, N. Seguin, Relaxation models of phase transition flows, ESAIM: Mathematical Modelling and Numerical Analysis 40 (2) (2006) 331–352.
URL https://hal.archives-ouvertes.fr/hal-00139607

[32] G. Faccanoni, H. Mathis, Admissible Equations of State for Immiscible and Miscible Mixtures, ESAIM: Proceedings and Surveys (2019).
URL https://hal.archives-ouvertes.fr/tel-00363460

[33] S. Jaouen, Etude mathématique et numérique de stabilité pour des modeles hydrodynamiques avec transition de phase, Ph.D. thesis, Paris 6 (2001).

[34] P. Helluy, Simulation numérique des écoulements multiphasiques: de la théorie aux applications, Habilitation à diriger des recherches, Université du Sud Toulon Var (2005).
URL https://tel.archives-ouvertes.fr/tel-00657839

[35] H. Mathis, Theoretical and numerical study of phase transition flows, Ph.D. thesis, Université de Strasbourg (Sep. 2010).
URL https://tel.archives-ouvertes.fr/tel-00516683

[36] R. Lewandowski, B. Mohammadi, Existence and positivity results for the φ- θ and a modified k- ε two-equation turbulence models, Mathematical Models and Methods in Applied Sciences 3 (02) (1993) 195–215. doi:https://doi.org/10.1142/S0218202593000114.

[37] L. Quibel, Simulation d'écoulements diphasiques eau-vapeur avec un modèle homogène, PhD, Université de Strasbourg.
URL https://tel.archives-ouvertes.fr/tel-02941486

[38] J.-P. Croisille, Contribution à l'étude théorique et à l'approximation par éléments finis du système hyperbolique de la dynamique des gaz multidimensionnelle et multiespèces, Ph.D. thesis, Paris 6 (1990).

[39] O. Hurisse, Application of an homogeneous model to simulate the heating of two-phase flows, International Journal on Finite Volumes 11 (2014) http://www.latp.univ–mrs.fr/IJFV/spip.php?article52.
URL https://hal.archives-ouvertes.fr/hal-01114808

[40] W. Wagner, H.-J. Kretzschmar, International Steam Tables: Properties of Water and Steam Based on the Industrial Formulation IAPWS-IF97, Springer-Verlag Berlin Heidelberg, 2008. doi:10.1007/978-3-540-74234-0.

[41] F. Daude, P. Galon, Z. Gao, E. Blaud, Numerical experiments using a hllc-type scheme with ale formulation for compressible two-phase flows five-equation models with phase transition, Computers & Fluids 94 (2014) 112–138. doi:https://doi.org/10.1016/j.compfluid.2014.02.008.

[42] N. Yanenko, Méthode à pas fractionnaires: résolutions de problèmes polydimensionnels de physique mathématique, Collection Intersciences, A. Colin, 1968.
URL https://books.google.fr/books?id=JBIyvgAACAAJ

[43] V. V. Rusanov, The calculation of the interaction of non-stationary shock waves with barriers, Zhurnal Vychislitel'noi Matematiki i Matematicheskoi Fiziki 1 (2) (1961) 267–279. doi:https://doi.org/10.1016/0041-5553(62)90062-9.

[44] C. Chalons, J.-F. Coulombel, Relaxation approximation of the euler equations, Journal of Mathematical Analysis and Applications 348 (2) (2008) 872 – 893.
URL https://hal.archives-ouvertes.fr/hal-01838843

[45] P. Helluy, O. Hurisse, E. Le Coupanec, Verification of a two-phase flow code based on an homogeneous model, International Journal on Finite Volumes 13 (Nov. 2016).
URL https://hal.archives-ouvertes.fr/hal-01396200

[46] B. Riegel, Contribution à l'étude de la décompression d'une capacité en régime diphasique, Ph.D. thesis (1978).

[47] O. Hurisse, L. Quibel, Simulations of a simplified LOCA scenario with a non-equilibrium homogeneous model (2020).
URL https://hal.archives-ouvertes.fr/hal-02901408

[48] F. Caupin, E. Herbert, Cavitation in water: a review, Comptes Rendus Physique 7 (9-10) (2006) 1000–1017. doi:https://doi.org/10.1016/j.crhy.2006.10.015.

[49] H. J. Maris, Introduction to the physics of nucleation, Comptes Rendus Physique 7 (9-10) (2006) 946–958. doi:https://doi.org/10.1016/j.crhy.2006.10.019.

[50] T. Petrova, R. Dooley, Revised release on surface tension of ordinary water substance, Proceedings of the International Association for the Properties of Water and Steam, Moscow, Russia (2014) 23–27.
URL http://www.iapws.org/relguide/Surf-H2O-2014.pdf